Two-photon optogenetics

Dan Oron, Eirini Papagiakoumou, Francesca Anselmi, Valentina Emiliani

Two-photon optogenetics

Dan Oron[1], Eirini Papagiakoumou[2], F. Anselmi[2] and Valentina Emiliani[2*]

[1]Department of physics of complex systems, Weizmann institute of science, Rehovot 76100, Israel

[2]Neurophysiology and New Microscopies Laboratory, Wavefront engineering microscopy group, CNRS UMR 8154, INSERM U603, Paris Descartes University, 45 Rue des Saints Pères, 75270 Paris Cedex 06, France

*corresponding author:
Tel: +33-142864253; e-mail: valentina.emiliani@parisdescartes.fr

Authors' additional information:

Dr. Dan Oron, Tel: 972-8-9346282, Fax: 972-8-9344109
e-mail: dan.oron@weizmann.ac.il
Dr. Eirini Papagiakoumou
Tel: +33-142864371, Fax: +33-142864255
e-mail: eirini.papagiakoumou@parisdescartes.fr
Francesca Anselmi
Tel: +33-142864371, Fax: +33-142864255
e-mail: francesca.anselmi@parisdescartes.fr

Keywords: optogenetics, photoactivation, light patterning, digital holography, temporal focusing, generalized phase contrast

Color figures: 12

Abstract

The use of optogenetics, the technology that combines genetic and optical methods to monitor and control the activity of specific cell populations, is now widely adopted in neuroscience. The development of optogenetic tools, such as natural photosensitive ion channels and pumps or calcium and voltage sensitive proteins, has been growing tremendously during the last ten years, thanks to the improvement of their performances in terms of facilitating light-stimulation. To this aim, efficient illumination methods are also needed. The most common way to photostimulate optogenetic tools has been, so far, widefield illumination with visible light. However, the necessity of addressing the complexity of brain architecture has recently imposed

switching to the use of two-photon excitation, which provides a better spatial specificity and deeper penetration in scattering tissue. Two-photon excitation is still challenging, due to intrinsic characteristics of optogenetic tools (e.g. the low conductivity of light-sensitive channels), and efficient illumination methods are therefore essential for advancing in this domain. Here we present a review on the existing two-photon optical approaches, applied for photoactivation of optogenetic tools, and future perspectives for the widespread implementation of these techniques.

1. Introduction

To achieve an efficient control of brain activity with light, precise spatiotemporal stimulation of neuronal structures is a fundamental requirement. In this respect, optogenetic tools (e.g. light-gated ion channels and pumps for photoactivation, or calcium and voltage sensitive fluorescent proteins, C/VSFPs, for functional imaging) have an important advantage over synthetic optical reporters because their expression can be restricted to a specific neuronal population by genetic targeting (Kramer et al., 2009). This has allowed loosening some constraints on illumination specificity, so that many neurobiological studies have been performed with one-photon (1P) widefield excitation, which has the advantage of technical simplicity. In the case of photoactivation, the low-power density necessary for 1P stimulation of optogenetic ion channels and pumps (e.g. 1 $mW \cdot mm^{-2}$ for generating action potentials with the light-gated ion channel channelrhodopsin-2 – ChR2, (Aravanis et al., 2007)) has permitted to stimulate deep into scattering brain tissues with widefield visible light, both *in vitro* (Arenkiel et al., 2007; Wang et al., 2007; Petreanu et al., 2009) and *in vivo* (Cardin et al., 2009; Gradinaru et al., 2009; Witten et al., 2010). As for functional fluorescence imaging, widefield illumination, together with the use of rapid CCD cameras, allows fast (> kHz) optical recordings and the possibility of averaging signals spatially over large surfaces (e.g. a cell soma or a portion of dendrite), thus increasing the number of collected photons. This is particularly important in the case of voltage imaging (Peterka *et al.*, 2011), where dynamics are often in the order of the millisecond, and the collected fluorescent signal can be small (relative fluorescent increase ~1 % per 100 mV for VSFPs in brain slices (Akemann et al., 2010; Mutoh et al., 2011)). Indeed optogenetic voltage imaging in neuronal preparations has been mostly performed with 1P widefield excitation, allowing to record neuronal activity both *in vitro* and *in vivo* (Chanda et al., 2005; Akemann et al., 2010).

Despite the impact of these results, widefield illumination for optogenetics presents some important limitations. When used for photoactivation, it does not allow stimulating a subpopulation of genetically identical neurons (a configuration which could be useful, for example, to mimic sparse physiological activity patterns), or targeting subcellular compartments, such as dendritic and axonal branches, or dendritic spines. Similarly, in widefield imaging, the signal form a region of interest is contaminated by aspecific fluorescence coming from out-of-focus planes and blurred by scattering, making it sometimes difficult to isolate contributions from a single cell body or dendrite, and decreasing the signal to noise ratio (SNR).

To address these issues spatial shaping of the illumination light (light patterning) is required. For 1P photoactivation, laser scanning approaches have been used to map functional neuronal connectivity, by successively stimulating different ChR2-expressing targets in brain slices (Petreanu et al., 2007; Wang et al., 2007; Petreanu et al., 2009). Alternatively, extended illumination patterns have been generated by using micro-Light Emitting Diode (LED) arrays as light sources or by inserting Digital Micro-mirror Devices (DMDs) in the widefield excitation path (intensity modulation). In these cases the patterns are imaged onto the sample plane by a telescope (generally formed by the microscope objective and tube lens): illumination profiles are generated by creating “dark regions” on the excitation field, either by deviating part of the excitation light outside the optical path (DMDs), or by turning off the corresponding emitters (micro-LED arrays). Intensity modulation techniques have been used both *in vitro* and *in vivo*, for example to photoactivate ChR2 expressing retinal ganglion cells (Farah et al., 2007; Grossman et al., 2010), to study the central pattern generator for locomotion (Wyart et al., 2009) and to probe odor coding mechanisms in the olfactory bulb (Dhawale et al., 2010).

Still, these approaches remain limited by intrinsic drawbacks of 1P illumination. In particular, the precision of excitation is hindered by the lack of axial resolution, which is often incompatible with single-cell selectivity or with stimulating thin neuronal processes. Moreover, visible light is highly scattered by living tissues, thus limiting the penetration depth and, in the case of imaging, decreasing the SNR.

Two-photon (2P) optogenetics has the potentiality to solve these problems, thanks to the inherent optical sectioning capability of 2P excitation (2PE) and the increased robustness to scattering of the longer wavelength used in that case.

1. Two-photon Optogenetics: illumination methods

A common challenge for 2P optogenetics is the need to enlarge the excitation surface. For photoactivation, this problem was first highlighted by Rickgauer and Tank, in the case of ChR2 (Rickgauer and Tank 2009). Indeed ChR2 has low single channel conductance (~80 fS (Feldbauer et al., 2009)). As a consequence, the depolarization induced by photostimulating ChR2 channels comprised into the volume of a standard 2P diffraction-limited spot is not big enough to exceed the threshold for action potential generation in neurons. Moreover, the relatively high 2P absorption cross section of ChR2 (~260 Goeppert-Mayer units at 920 nm, (Rickgauer and Tank 2009)) and the long lifetime of the excited states (~ 10 ms) cause fast saturation of the channels, preventing the increment of neuronal depolarization by simply raising the excitation power. Similarly, for 2P voltage imaging, the membrane surface, and so the number of reporter molecules, which can be excited by a 2P spot is small and, consequently, the SNR is low (*shot-noise* $\propto$ square root of the collected fluorescent photons).

To improve the efficiency of 2P stimulation, the solution is then to extend the excitation area. This might be achieved with different approaches that can be divided in two main groups: scanning and parallel excitation techniques. In the first case, the excitation area is increased by rapidly steering the laser beam through different positions on the target structure, while, in the second case, larger excitation spots are generated by modulating the phase of the illumination laser beam.

2.1 Scanning approaches

The first demonstration of 2P activation of ChR2 was performed by D. Tank's group (Rickgauer and Tank 2009). Two configurations to increase the excitation area were compared. In the first one, the laser spot diameter was enlarged by underfilling the back aperture of the microscope objective. This was effective in increasing the size of ChR2-evoked currents, but caused a degradation of axial resolution, since it reduced the effective numerical aperture (NA) of the microscope objective. In the second case, the 2PE spot was scanned across different positions on the target cell. In this configuration, ChR2-evoked currents from regions stimulated sequentially would sum up, contributing to the final response. The scan time, T_s, was limited by the decay time constant, τ_d, of ChR2 currents ($I^*(T_s)/I^*_{max} = (1-e^{-n})/n$, with $n=T_s/\tau_d$, where I^* is the evoked photocurrent and I^*_{max} is the maximal available current through ChR2 channels in the conductive state (*); (Rickgauer and Tank

2009)). A combination of the two approaches led to the first successful attempt to stimulate action potentials by 2P activation of cultured hippocampal neurons transfected with ChR2 (Fig.1). The microscope objective was slightly underfilled to give an effective NA of 0.2-0.5 (corresponding to an axial profile covering, approximately, the thickness of the cell). Then the excitation spot was scanned along spiral trajectories on the neuronal soma: an action potential could be generated with a scan time of ~ 30 ms. This is still limited in terms of temporal resolution: in particular, the technique is not suitable for "simultaneous" (within a few milliseconds) stimulation of multiple cells, as it is necessary to mimic fast spontaneous neuronal circuit activity. Nevertheless, these results opened the way to 2P optogenetics.

To date, no data are available, to our knowledge, on 2P imaging with VSFPs, but some studies have been performed with synthetic voltage-sensitive dyes (VSDs). In these works, as in the case of ChR2, rapid laser scanning was used to extend the area of excited membrane. For example, 2P laser scanning over a short line (3 points, ~0.5 μm, 100 μs per point) was used to perform voltage imaging on small (μm) axonal terminals in a neurohypophysis preparation *in vitro* (Fisher et al., 2008): action potentials and action potential trains were visualized in single trials, with a relative fluorescence increase up to 10% (di-3-ANEPPDHQ dye, 10-20 mW at the sample). 2P voltage imaging (ANNIE-6 dye) was also used with living mice, to monitor global changes of membrane potential in the upper layers of the somatosensory cortex, following whisker deflection, or during the transition from the anesthetized to the awake state (Kuhn et al., 2008): the laser spot was scanned over a line crossing an entire cortical column (~ 200 μm, 0.8 ms); the signal was averaged spatially and temporally (over 400 trials, relative fluorescence increase ≤ 1%). These preliminary results seem to indicate that 2P voltage imaging on enlarged areas is a promising research line to be pursued and, possibly, extended to the use of VSFPs.

2.2 Parallel approaches

2.2.1 Lateral shaping: digital holography and generalized phase contrast method.

For 2P parallel light patterning, methods based on intensity modulation of the illumination light are far too inefficient, so the only option is to use phase modulation. This can be achieved either by the use of static beam multiplexing (Nikolenko et al., 2007) or of reconfigurable liquid crystal devices. In the latter, two

approaches have been proposed: one is based on the principle of Digital Holography (DH) (Curtis et al., 2002), the second on the Generalized Phase Contrast method (GPC) (Glückstad and Mogensen 2001).

One-photon and two-photon digital holography

Originally proposed for generating multiple optical tweezers (Reicherter et al., 1999; Curtis et al., 2002), the experimental scheme for DH consists in computing, with an iterative algorithm, the phase pattern at the rear aperture of the objective that permits to reproduce the desired target intensity in the objective focal plane. The calculated phase-hologram is addressed to a liquid crystal spatial light modulator (LC-SLM) that is designed to impose the phase modulation onto the input beam's wavefront. After propagation through the objective, the beam is focused onto an intensity pattern, reproducing the desired template (Fig. 2a).

For multiple spot generation a simple algorithm called '*gratings and lenses*' (Liesener et al., 2000; Leach et al., 2006) can be used. This consists in imposing a grating effect to control the lateral position of each spot and a lens effect to control the axial position (Fig. 3). This algorithm is of easy implementation but does not permit to control the relative intensity of the spots at the focal plane (Liesener et al., 2000; Leach et al., 2006) and significant intensity inhomogeneity can be observed for the generation of a high number of spots.

To improve multiple-spot light distribution or to generate arbitrary two-dimension (2D) intensity distributions, the holographic phase at the SLM is normally calculated with another algorithm called the Gerchberg and Saxton algorithm (Gerchberg and Saxton 1972) (Fig. 2b), or with an improved version of it known as Gerchberg-Saxton Weighted (GSW) algorithm, which is particularly suited for optimizing uniformity in multiple diffraction-limited spots (Di Leonardo et al., 2007).

With these approaches, generation of multiple photoactivation spots in 2D (Lutz et al., 2008; Nikolenko et al., 2008; Nikolenko et al., 2010) or three-dimensional (3D) patterns (Daria et al., 2009; Anselmi et al., 2011; Yang et al., 2011) has been demonstrated. It has also been shown that, by designing the target intensity profile on the base of a fluorescence picture, light excitation can be shaped to perfectly match a specific subcellular process (Lutz et al., 2008; Dal Maschio et al., 2010), a cell soma (Zahid et al., 2010) or a defined group of cells (Zahid et al., 2010; Dal Maschio et al., 2010) (Fig. 4). Interestingly, for 2D shaped patterns the

spatial phase distribution of a holographic wavefront permits also improved axial resolution (Fig. 5).

An important parameter to be taken into account when designing a holographic system is the maximum lateral size of the excitation area. Accordingly to previous papers, e.g. (Golan et al., 2009), we can adopt for that the term field-of-view (FOV), normally used for imaging systems. In DH the FOV is mainly limited by the SLM pixel size, $d_{SLM,}$ which sets the maximum achievable deflection angle and gives rise to a position (x,y) dependent diffraction efficiency, $\delta(x,y)$, defined as the ratio between the intensity, I_{spot}, redirected into the desired target spot(s) and the light intensity, I_{tot}, incident on the LC-SLM, i.e. $\delta(x,y) = I_{spot}(x,y)/I_{tot}$ (we neglect for simplicity the losses due to the optical elements of the light path). Inside the FOV, $\delta(x,y)$ decreases proportionally to: $\delta(x,y)_{DH} = \left(\frac{\sin X}{X}\right)^2 \left(\frac{\sin Y}{Y}\right)^2$ (Golan et al., 2009; Yang et al., 2011), where: $X = \left(\frac{\pi f_2 d_{SLM}}{\lambda f_1 f_{obj}} x\right)$, $Y = \left(\frac{\pi f_2 d_{SLM}}{\lambda f_1 f_{obj}} y\right)$, and reaches a zero value at $x_{max} = y_{max} = 2 \times \left(\frac{\lambda f_1}{d_{SLM}} \frac{f_{obj}}{f_2}\right)$, where λ is the wavelength used, f_1/f_2 is the telescope magnification (typically ~1.5), f_{obj} is the objective focal lens and $1/2d_{SLM}$ is the maximum SLM spatial frequency (typically ~25 lp/mm). In 2PE one has to take into account the quadratic dependence of the signal from the excitation density so that the generated signal decreases to zero proportionally to $\left(\frac{\sin X}{X}\right)^4 \left(\frac{\sin Y}{Y}\right)^4$; for example for a diffraction efficiency ≥ 50% (spatial frequency of ~25 lp/mm), λ=900 nm, and an objective of 60x, 40x or 20x the FOV_{2PE} (FOV= $2x_{max} \times 2y_{max}$) in 2PE is of ~ 80x80, 120x120 or 240x240 μm^2, respectively.

To date, 1P and 2P holographic photostimulation have been applied for glutamate uncaging and imaging, however we anticipate that the extension to optogenetics will be straightforward. By combining 1P or 2P holographic photoactivation with electrophysiological recordings or calcium imaging, it has been possible to show that patterned excitation allows for a precise control of glutamate release in single (Lutz et al., 2008; Anselmi et al., 2011) and multiple (Yang et al., 2011) subcellular processes or in single and multiple neurons (Lutz et al., 2008; Nikolenko et al., 2008; Dal Maschio et al., 2010; Zahid et al., 2010; Fig.6).

Alternatively, holographic light patterning was used to illuminate specific regions of interest (ROIs) within the FOV, while performing conventional galvo-steered uncaging of MNI-glutamate (Dal Maschio et al., 2010) (Fig. 6). This configuration permits to integrate the calcium response on large ROIs and thus to significantly increase the SNR.

One limitation of DH is the inhomogeneous light distribution within the generated light patterns. This can be of the order of 15-20% for 1P excitation (1PE), while for 2PE, due to the quadratic dependence of the signal on the excitation density, it can reach a value of ~50% (see *x,y* light distribution in Fig.3 and Fig.4).

These fluctuations, also called intensity speckles, rise principally from the approximation in the iterative algorithm (since the problem of obtaining a desired intensity pattern in the Fourier plane by using only phase modulation does not usually have a solution, the output intensity is optimized by leaving a random phase distribution at the focal plane (Fig. 2b)) and from the cross talk of adjacent pixels of the LC-SLM (Guillon et al., in preparation). Solutions based on using a rotating diffuser (Papagiakoumou et al., 2008) or phase mask shift-averaging (Golan and Shoham 2009) permit averaging over the speckles and lead to a smoother spatial distribution. However, in the case of a diffuser this causes a significant loss of light and a deterioration of the axial resolution. The shift-averaging methods require projecting a series of holograms, and are thus limited by the refresh rate of the LC-SLM (60-200 Hz); this can be reduced by using binary ferroelectric LCs (which can get up to the kHz range). Unfortunately at present these devices have a very poor efficiency (15-20%).

The presence of speckles is not critical in applications using holographic illumination for recording the integrated signal from a defined ROI (Dal Maschio et al., 2010) or for uncaging on large areas (the diffusion of the uncaged molecule quickly smooths out the speckle distribution after the end of the stimulation). Nevertheless, for applications requiring a precise control of light excitation on fine subcellular processes or a precise quantification of the excitation, one should consider using alternative schemes for light patterning, such as the Generalized Phase Contrast (GPC) method described in the following paragraph.

Principle of the Generalized Phase Contrast Method

The GPC method is based on an extension of the Zernike phase-contrast method (Zernike 1955) into the domain of full range [0, 2π] phase-modulation

(Glückstad 1996; Rhodes 2009). Briefly, a desired target intensity map is converted into a binary [0, π] phase map that is used to modify the input beam wavefront via a LC-SLM. The beam modulated by the LC-SLM is then focused on a patterned Phase Contrast Filter (PCF) plate that imposes appropriate phase retardation between the on-axis focused component (reference wave) and the higher-order Fourier components (signal wave, focused around the central spot). The interference between these two beams generates, at the focal plane of a second lens (the output plane), the original target intensity (Fig. 7a, top).

GPC has been initially introduced to realize optical tweezers (Rodrigo et al., 2004) and recently adapted to generate shaped 2PE patterns (Fig. 7a, bottom) (Papagiakoumou et al., 2010). In the latter, it has been shown that, by addressing the LC-SLM with binary phase map conversion of a user defined ROI in a fluorescence image, it is possible to precisely reproduce the original intensity target (Fig. 7b). Contrary to the case of DH, in GPC the optical wavefront at the objective's back aperture and at the focal plane is flat. This allows on one hand the generation of sharp, speckle-free patterns (Fig. 7b) but gives rise, on the other hand, to the loss of optical confinement (the axial propagation of a GPC beam being very similar to the one of low-NA Gaussian beams) (Fig. 7c).

In GPC, the FOV is given by the circular illuminated area at the SLM (of radius *Rc*) multiplied by the magnification of the GPC interferogram and the relay telescope $\mathrm{FOV}_{GPC} = \pi \cdot \left(Rc \cdot \frac{f_2}{f_1} \frac{f_{obj}}{f} \right)^2$, where f_1 and f_2 are the focal lengths of the corresponding lenses in the GPC setup (Fig. 7a, bottom), and f and f_{obj} are the focal lengths of the telescope forming the final intensity pattern at the objective's focal plane (Lens 3 and objective). Although, in this case, it is more appropriate to talk about a phase interferometric contrasting, we will keep for δ the denotation "diffraction efficiency" for similitude to the case of DH.

Two parameters determine the value of δ within the FOV. The first one is the ratio, $S = A_{\mathrm{spot}}/\mathrm{FOV}$ of the excitation pattern area, A_{spot}, to the FOV: it can be demonstrated that, for $S = 0.25$ (i.e. $A_{spot}(\max) = \mathrm{FOV}/4$), δ reaches its theoretical maximum value of 100% (Palima and Glückstad 2008). However, for smaller excitation areas it decreases proportionally to the ratio $A_{spot}/A_{spot}(\max)$.

Secondly, the spatial dependence of δ within the FOV is given by the central filtering size, η, defined as the ratio between the diameter of the PCF, R_1, to the main

lobe of the Airy profile of the reference wave focused at the PCF plane, R_2 - i.e. the Fourier transform of the input circular aperture of radius R_c (Glückstad and Mogensen 2001). This parameter determines the strength and the wavefront curvature of the reference wave at the GPC output aperture and therefore, implicitly, the diffraction efficiency δ in the FOV (Glückstad and Mogensen 2001). In general a value of η between 0.5 and 0.6 represents a good compromise between wavefront curvature and strength of the synthetic reference wave, i.e. between FOV and intensity contrast. We can include the dependence of the diffraction efficiency on the two parameters, η and *S*, by defining the total diffraction efficiency for binary input phase GPC: $\delta_{GPC} = I_{spot}/I_{tot} = \delta_\eta \cdot 4\frac{A_{spot}}{FOV}$; for $A_{\text{spot}} \leq \frac{\text{FOV}}{4}$; where *r* is the radial coordinate at the excitation plane and ΔR is the excitation field radius.

2.2.2 Axial shaping: temporal focusing

As is evident from Fig. 5 and Fig. 7c, the rules of diffraction practically determine a relation between the lateral excitation shape and its axial extent. For flat wavefronts (Fig. 4a, Fig.6c), the axial extent scales quadratically with the lateral size (Goodman 2005). Holographic excitation (Fig. 5b), which utilizes the full angular acceptance ('numerical aperture') of the excitation lens, enables to achieve a linear scaling between the two, but at the price of adding significant speckle to the lateral pattern (Fig. 5b,c). These restrictions seem to be an insurmountable barrier for generating large area axially confined excitation patterns. For 2PE, however, various alternatives for illuminating large areas, while maintaining axial confinement, are available, taking advantage of temporal multiplexing (i.e. exciting different points within the FOV at different times). This can be achieved by fast scanning of a single excitation point, but the finite residence and traveling time required limits the number of positions that can be considered 'simultaneously' activated on a biological timescale.

Provided that the excitation source is powerful enough, axially resolved spatial multiplexing can also be achieved by splitting the beam into several beamlets, time delayed (10 ps) relative to one another and directed at different spatial locations (Fricke and Nielsen 2005). Going to a large number of beamlets, though, their separate control becomes cumbersome, making this approach difficult to scale beyond several tens of beamlets.

Several years ago, temporal focusing (TF) has been suggested as a continuous, easily controlled, alternative to the use of a discrete number of beamlets for multipoint excitation. TF is a technique based on imaging the required excitation pattern onto the sample. The standard temporal focusing setup is depicted in Fig. 8, and consists of a grating which is imaged onto the sample via a 2f-2f telescope consisting of an achromatic lens and the microscope objective. Since this is a perfect imaging system, the pattern illuminating the grating is simply demagnified and relayed onto the objective focal plane. To understand why axial resolution is maintained in this configuration it is instructive to consider the time-domain evolution of a short pulse impinging upon the grating. For ultrafast excitation the incoming pulse of duration, τ, is pancake-shaped, covering a relatively large transverse area, but having a thickness of only $c\tau$ (where c is the speed of light), corresponding to about 30 μm for 100 fs pulses, typically used for multiphoton excitation. Since light scattered from the grating is diffracted onto the first order, the illuminating pulse has to impinge upon the grating at an angle. Thus, different regions of the grating are *not illuminated simultaneously.* Transiently, only the intersection between the pancake-shaped pulse and the grating surface, which is an extended line along the grating grooves, is illuminated. Upon proper choice of the grating and telescope parameters, this line is imaged onto a diffraction-limited line in the objective focal plane. Considering all this, TF can be viewed as temporally multiplexed line-scanning multiphoton excitation. Indeed, for widefield temporally focused excitation, the axial resolution, $2\Delta z_0$, defined as the full width at half maximum (FWHM) of the axial intensity distribution, I_{2P}, has been shown to be equivalent to that of multiphoton line-scanning microscopy both for multiphoton absorption (Oron et al., 2005) and for coherent nonlinear processes such as multiharmonic generation (Oron and Silberberg 2005): $I_{2P} \approx \left[1+\left(\frac{\Delta z}{z_R}\right)^2\right]^{-0.5}$; $2\cdot\Delta z_0 = 2\sqrt{3}z_R$, where z_R is the Rayleigh range.

Two clear consequences follow from the above description. The first is that as long as the pulse front is not distorted, TF affords to maintain the axial resolution regardless of the particular shape of the excitation pattern, and that axial resolution should only slowly deteriorate for weakly distorted pulses. The second is that axial resolution is improved if the excitation pattern on the grating is shaped as a thin line perpendicular to the grating grooves (Tal et al., 2005; Zhu et al., 2005). In this case,

the instantaneous intersection of the pulse with the grating is a small area, which is imaged onto a diffraction-limited spot in the objective focal plane, and the axial resolution, would be equivalent to that of a conventional 2P microscope:

$$I_{2P} \approx \left[1+\left(\frac{\Delta z}{z_R}\right)^2\right]^{-1}; 2\cdot\Delta z_0 = 2z_R.$$

It should be noted here that a complementary description of TF in the frequency domain exists. It relies on the fact that the various colors comprising the ultrashort excitation pulse are diffracted by the grating towards different directions and thus propagate towards the objective focal plane at different angles. This leads to axially dependent spectral dispersion, so that the pulse is temporally stretched outside the focal plane. As a result, multiphoton excitation is axially confined. While less intuitive than the time-domain description, the frequency domain one is sometimes useful to understand the physics behind the evolution of temporally focused pulses, for example in the cases of remote focusing or of transmission through scattering media, as described below.

The frequency domain is also useful to provide an alternative description why TF enables to decouple the lateral and axial resolution. For a conventional Gaussian illumination the Rayleigh range, z_R, depends quadratically on the excitation spot size, w_0, or on the inverse of the square of the beam NA:

$$z_R = \pi w_0^2/2\lambda \propto \lambda/\mathrm{NA}^2 \qquad (1),$$

where NA$=s/2f$, f is the objective focal length and s is the size of the illuminating beam at the objective back aperture (equal in the x and y directions). For a diffraction-limited spot, s is larger than the objective back aperture, D, (overfilling) and NA in equation (1) coincides to the objective NA, $\mathrm{NA}_{obj} = D/2f$. Increasing the size w_0 of the spot at the focal plane requires decreasing s and consequently NA, so that NA becomes less than NA_{obj} and the axial resolution decreases, as well. For a temporally focused beam $z_R = \frac{2f^2}{k(s^2+\alpha^2\Omega^2)}$ (Durst et al., 2006), where k is the mean magnitude of the excitation wave vector and s and $\alpha\Omega$ are the spot sizes at the back aperture of the objective in the direction orthogonal and parallel to the grating linear dispersion, respectively. As for the case of conventional Gaussian beams, the generation of large excitation spots at the focal plane requires reducing s but this affects the back aperture illumination only in one direction, the other being always

equal to $\alpha\Omega$; for $\alpha\Omega > D$ and a large excitation area, $s \ll \alpha\Omega$ and $z_R \approx \frac{2f^2}{k(\alpha^2\Omega^2)} = \frac{\lambda}{\mathrm{NA}_{obj}^2} = const$. In this regime, the axial resolution depends only on the NA_{obj} independently of the excitation spot size, w_0. In other words w_0 can be increased without sacrifying the NA of the system and therefore without losses in axial resolution. This leads to an effective decoupling of the axial and lateral beam parameters.

2.2.3 3D sculpting: lateral and axial shaping

The fact that TF is practically an imaging technique greatly facilitates its use for generating complex spatial excitation patterns. As long as it does not lead to significant distortion of the pulse front, any phase modulation technique can be used to generate the required magnified image on the grating. This image will then be relayed onto the sample resulting in an axially resolved excitation pattern. In particular, both wavefront shaping methods described above, DH and GPC, can be easily integrated with TF.

TF was first combined with wavefront shaping by Papagiakoumou and coworkers in 2008 (Papagiakoumou et al., 2008; Papagiakoumou et al., 2009), who coupled it with a standard DH setup. A phase-only LC-SLM was placed at the focal plane of a lens positioned one focal length away from the grating. Thus, the image on the grating was the Fourier transform of the phase pattern applied to the SLM. To obtain the desired image, a Gerchberg-Saxton iterative optimization algorithm was used.

Two years later TF was combined with GPC, in this case the grating was placed at the output plane of the GPC interferometer (Fig. 9a) (Papagiakoumou et al., 2010).

In both cases an axial resolution close to the theoretical limit for temporal focusing has been demonstrated (Fig. 9b). It should be noted that due to the inherent distortion of the pulse front in the case of DH, there is a slight deterioration of the axial resolution as compared with GPC, which is well accounted for by theoretical calculations (Papagiakoumou et al., 2008; Papagiakoumou et al., 2009).

The combination of GPC and TF has been used for efficient in-depth 2P-activation of ChR2 in cultured neurons and brain slices (Papagiakoumou et al.,

2010), enabling action potential generation with 2-ms temporal resolution (Fig. 10a) and ~5 μm axial resolution (Fig. 10b) and, for the first time, reliable generation of action potentials with the simultaneous excitation of multiple neurons (Fig. 10a) or multiple neuronal compartments (Papagiakoumou et al., 2010).

Alternatively to these approaches, enlarged and optical confined excitation area for 2P-activation of ChR2 can be achieved by using a low-NA Gaussian beam in combination with TF, as demonstrated by Andrasfalvy et al. (Andrasfalvy et al., 2010). In this case excitation patterns that match the shape of neuronal processes (Andrasfalvy et al., 2010) or of a targeted neuronal population (Losonczy et al., 2010), were achieved by integrating the technique into a laser scanning head. Action potentials from a single dendrite in acute brain slices could be triggered at ~150 μm depth by placing multiple spots along the dendrite (Andrasfalvy et al., 2010) with ~ 6 ms temporal resolution. The same approach has allowed to study the underlying mechanisms of theta phase precession by inducing spatiotemporal patterns that mimic the perisomatic inhibition on hippocampal pyramidal cells (Losonczy et al., 2010).

2.4 Comparison between the different approaches

Overall each of the above approaches has certain advantages and limits and, as a result, each of them might prove to be best suited in a given experimental setting (see also (Vaziri and Emiliani 2011)). These are briefly described in this paragraph and summarized in Table 1.

The spiral scanning approach proposed by J.P. Rickgauer and D. Tank (Rickgauer and Tank 2009) can be easily implemented, since it only requires the introduction, in a conventional microscope, of an iris at the objective back aperture or of a variable beam expander in the excitation optical path, to reduce the effective NA of the objective. All the available power can be concentrated in a single spot scanned trough the sample. The FOV is the one of a conventional scanning microscope, i.e. FOV=$2 \cdot f_{scan} \cdot \tan(\vartheta) \cdot M$, where f_{scan} is the focal length of the scanning lens, ϑ the galvo-scanning angle (typically ±11°) and M the objective magnification; this leads, for example, to a FOV of ~600x600 μm^2 for a 40x objective.

The main limitation of this approach is that a compromise between axial and temporal, T_S, resolution has to be found. The latter is given by:$T_S = N(t_{dwell} + S_t)$, where N is the number of visited positions during the scan, which is given by the

ratio between the total excited area of the pattern, A_{Spot}, and the excitation spot size, w_0; t_{dwell} is the residence time at a given position (also known as dwell time) and S_t the point to point scanning time. Increasing the temporal resolution requires increasing w_0, with consequent deterioration of the axial : $R_z \propto w_0^2$. This approach is therefore particularly suitable for single cell stimulation, but generation of high frequency action potential trains or ms excitation of multiple cells are not possible.

Scanning of a temporally focused low-NA beam, as proposed by Andrasfalvy et al. (Andrasfalvy et al., 2010), allows for increasing w_0 without deteriorating the axial resolution, which remains equal to $\frac{\lambda}{\mathrm{NA}_{obj}^2} = const$. The implementation of this approach is relatively easy (requiring adding a TF grating in the external optical path or inside the scanning head of a commercial 2P microscope).

In terms of light efficiency, one has to take into account the losses due to the diffraction at the TF grating (15-20%), and the fact that the remaining power is divided by the total excitation area A_{spot}. This is not a real limit for photoactivation of ChR2, considering the high 2P cross section of these channels. The situation is less clear with voltage imaging, since VSFPs have not yet been tested for 2PE. The FOV in that case is the same as for the spiral scanning approach.

For single spot excitation, this approach is limited to shape of circular symmetry and needs readjusting the spot size with a variable telescope for experiments requiring different excitation spots. For multiple-cell excitation or excitation of arbitrary patterns, it requires scanning the excitation beam. In this case the expression for the temporal resolution is the same as for the spiral scanning approach: $T_S = N(t_{dwell} + S_t)$. Nevertheless, the use of a temporally focused beam allows for larger values of w_0 and consequently for a better temporal resolution. However, for excitation of small processes (such as dendritic segments or axons), w_0 should be kept of the order of the lateral size of the processes (1-2 μm) so that the gain in temporal resolution with respect to the spiral scanning approach is less evident.

Overall this technique is well suitable for single cell excitation or multiple-cell excitation, provided that the number of excited cells is not too elevated or that a short d_{well} time is needed. A significant gain in temporal resolution can be also achieved by reducing the dwell time, i. e. by increasing the excitation power, however this costs in lateral and axial resolution due to the strong contribution of the

out-of-focus light to the evoked responses (Rickgauer and Tank 2009; Andrasfalvy et al., 2010; Losonczy et al., 2010).

Parallel light shaping with DH requires significant modifications of the optical setup with respect to a conventional 2P microscope, and an *ad hoc* software for the calculation of phase profiles.

In terms of light efficiency, in DH simultaneous stimulation of multiple areas implies that the available laser power is dived by the total excitation area, A_{spot}. This, in addition to the power losses at the LC-SLM (30%) and at the TF grating (15-20%) can limit the maximum number of excitable cells and the penetration depth.

The FOV is limited by the position-dependent diffraction efficiency of the SLM and is given by: FOV=$\left[2 \times \left(\left(\lambda f_{obj} f_1\right)/(2 d_{SLM} f_2)\right)\right]^2$; this, for a diffraction efficiency of ≥ 50% (~spatial frequency of ~10 lp/mm), λ=900 nm, and a 40x objective, corresponds to a FOV in 2PE of ~ 120x120 μm^2.

In comparison to scanning methods, the main advantage of DH is the temporal resolution which is only limited by the dwell time: $T_S = t_{dwell}$ and is independent of the number of excited positions.

Holographic light patterning also allows for efficient multiple-scale excitation, going from single or multiple diffraction-limited spots to shapes covering a single subcellular process or a population of sparse neurons, without any adjustments of the optical setup.

For excitation of a single cell, cell process, or multiple sparse cells, DH permits achieving an axial resolution ~10 μm (Lutz et al., 2008; Dal Maschio et al., 2010; Zahid et al., 2010) even without TF, thus allowing for a simpler optical setup and reduced power losses. With DH, 3D light-patterning is also possible, which is not achievable with any of the other described approaches (laser scanning or GPC methods).

Advantages and limitations for GPC are very close to those described for DH, with few differences. Similar to DH, parallel light shaping with GPC requires significant modifications of the optical setup, but the software for phase profile calculation, which consists in a simple intensity-binary phase conversion of the original target, is of easy implementation.

In terms of light efficiency, the diffraction efficiency at the LC-SLM can be raised to the theoretical limit of 100% providing that the total spot surface consists of ¼ of the excitation field: A_{spot} = FOV/4. However this also sets a limit on the

maximum excitation density achievable, given by the ratio between the available excitation power and ¼ of the excitation field, independently of the excitation spot size. This has limited the excitation field in practical applications to a circle of ~60-100 μm diameter (Papagiakoumou et al., 2010).

In GPC, as in DH, the temporal resolution is only limited by the dwell time $T_S = t_{dwell}$ and is independent of the number of excited positions. Multiple-scale excitation is possible, without affecting the temporal resolution or requiring modification of the optical setup.

In contrast with DH, GPC permits the generation of sharp speckle-free excitation patterns. This is particularly interesting for photoactivation of small cellular processes, permitting generation of patterns which precisely match the lateral size, e.g., of dendrites. The smooth light distribution achievable with TF-GPC makes it also particularly adapted for fast imaging, e.g. with VSD and VSFP.

For experiments requiring sequential excitation with phase modulation, the refresh rate, R_e (60-200Hz), of the LC-SLM has to be taken into account in the definition of temporal resolution. To this end, we can consider a more general expression for T_s, including the sequential projection of n patterns (supposing for simplicity that each pattern comprises the same number of spots):
$T_S = N(t_{dwell} + S_t) + 1/R_e$; which, for parallel approaches (N=1, S_t=0), gives $T_S = t_{dwell} + 1/R_e$ and, for scanning approaches ($1/R_e$=0), gives $T_S = N(t_{dwell} + S_t)$. Scanning approaches are therefore preferable with respect to parallel approaches when $N(t_{dwell} + S_t) \leq (t_{dwell} + 1/R_e)$.

2. 2P Optogenetics: Decoupling the imaging from the activation plane

The use of optogenetic photoactivation in combination with functional imaging will permit a full optical control of signal transmission in brain. Ideally, since many brain structures are organized in complex volumes, both imaging and photoactivation should be performed in 3D. Moreover, one should be able to choose the imaging and stimulation planes independently, even when both are combined (as it is often the case) into the same microscope objective. This would allow overcoming current technical limitations, which, for example, restrict the accessible areas for simultaneous imaging and photoactivation to the relatively short portion of a dendrite, which extends in the focal plane of the microscope (Judkewitz et al., 2006; Kwon and Sabatini 2011), or, in the case of functional mapping of circuit

connectivity, to neuronal bodies located on the same plane (Nikolenko et al., 2007). In the following paragraph we will describe three possible methods permitting to decouple the imaging from the photoactivation plane.

The first approach is based on the use of DH. As described in paragraph 2.2 and Fig. 11a, multiple holographic spots can be generated at axial positions different from the objective focal plane by using *the grating and lenses* algorithm or with the GSW algorithm. Arbitrary 2D patterns can also be displaced by adding a global lens effect to the phase hologram used to generate the 2D pattern (Zahid et al., 2010). In both cases, projection to the SLM of different phase holograms, each one introducing a variable lens effect, which compensates for the scanning objective movements, permits to perform 3D imaging while keeping the stimulation plane at a fixed position, as demonstrated few years ago for 3D optical trapping and imaging (Emiliani et al., 2006) (Fig. 11a). Very recently, 3D 2P imaging without moving the objective (Dal Maschio et al., 2011) by performing lateral scanning of the spot with a conventional 2P laser-scanning microscope and axial displacement of the spots holographically with a SLM: it has been shown that the system has little spatial and temporal distortion and its fluorescence imaging performances on cellular structures in the intact mouse brain were demonstrated. This approach, combined with phase-modulated light patterns (TF-DH or TF-GPC), will also permit to achieve a full decoupling of the stimulation and imaging planes.

TF offers yet another alternative for decoupling the excitation plane from the imaging plane. As described above, TF can be considered, in the frequency domain, as pulse shortening ('focusing' in time) during propagation up to the objective focal plane. In complete analogy with the lens effect in DH, addition of a quadratic spectral phase (rather than spatial phase as in DH) results in an axial shift of the focusing plane. Application of an appropriate amount of chirp, $\beta\Omega^2$ (quadratic spectral phase, 2β is the Group Velocity Dispersion (GVD) and $\sqrt{2ln2}\Omega$ is the FWHM of the frequency spectrum of the pulse) enables an arbitrary shift of the focal plane, $z_{foc} = f + \beta\Omega^2 z_R$, as long as the various colors comprising the ultrashort pulse are still spatially overlapping in the shifted plane (corresponding typically to several Rayleigh ranges of the objective lens, and depending on the transverse extension of the excitation beam) (Durst et al., 2006; Suchowski 2006) (Fig. 11b). This effect has been demonstrated in various realizations of imaging, and more

recently used for remote control of the axial focusing through an optical fiber (Straub et al., 2011).

Finally a third possibility proposed recently (Anselmi et al., 2011) consists in combining DH with a remote focusing imaging unit (Botcherby et al. 2007). In this system, photostimulation patterns are generated by DH through the principal microscope objective, as described above. 1P fluorescence imaging is carried out by a second microscope, symmetrical to the principal one, which recreates a perfect (aberration-free) 3D remote image of the sample. A mirror, in the remote space, is then used to move this image, in order to select the final imaging plane on the camera, which can be axially displaced with respect to the principal focal plane or tilted by a variable angle (up to ~20°). In this way, 3D imaging can be performed without actually translating the principal microscope objective, i.e. independently from photoactivation (Fig. 11c). This technique was first implemented for 1P fluorescence imaging, and excitation light, provided by a LED, was coupled to the principal objective through a conventional epifluorescence pathway (Anselmi et al., 2011). 1P glutamate uncaging was performed by implementing, in the same microscope, a system for DH. Remote focusing is also compatible with 2P imaging (Salter et al., 2009). In this case, the imaging laser is coupled directly into the remote unit: lateral scanning can be performed by a pair of galvanometers, while axial scanning can be carried out by the remote mirror associated to galvanometric motors (Botcherby et al., 2010).

3. 2P Optogenetics: Deep two-photon activation

Multiphoton excitation provides what is currently one of the best solutions for optical imaging and photoexcitation through scattering tissue. This relies on the fact that the scattered components of the excitation beam typically contribute little to multiphoton processes, as they are both weak and temporally stretched. Thus, the ballistic photons of the excitation beam induce most of the generated signal. The limitations of this technique are due to the fact that these ballistic photons are exponentially attenuated due to scattering during propagation through the sample, while focusing increases the generated signal only polynomially ($1/z$) with propagation. Thus, for too thick samples, the majority of the nonlinear signal no longer generates from the focal plane (Theer and Denk 2006).

The effect of scattering can be dramatically enhanced for multiple-point or temporally focused excitation, since in both cases the scattered excitation beam from

one illuminated spot can interfere with the ballistic photons from another. This can lead to a significant distortion of the excitation shape if the various excitation spots are not enough temporally separated one from the other. Moreover, scattering should lead, due to similar effects, to a decrease in axial resolution of photoactivation. Recent experimental and theoretical investigation of the propagation of temporal focused low-NA Gaussian beams (Dana and Shoham 2011), holographic beams, or beams generated with the GPC method through scattering tissue has characterized the deterioration of the axial resolution as a function of propagation distance. It was found that the axial resolution is roughly maintained up to about two scattering lengths, and quite rapidly deteriorates thereafter. Interestingly, the excitation shape was found to be extremely robust against scattering within a propagation distance of up to about two scattering lengths, such that even relatively fine features are preserved despite scattering. This latter effect can be understood in terms of the nearly independent speckle patterns induced by the scattering medium to each of the excitation colors comprising the temporally focused pulse, which tend to average out in the multiphoton response. This has enabled to adequately preserve the excitation pattern even upon propagation of about 0.5 mm in an acute brain slice (Fig. 12).

Outlook

To date, the use of optogenetics as a research tool in neuroscience grows rapidly. Fast and specific optical control opens a new landscape for studying neuronal systems, by permitting stimulation and imaging of neuronal populations. With respect to classical electrical techniques, optical methods are less invasive, have increased flexibility (for example in imaging and stimulating form multiple cells simultaneously), and allow direct access to small structures, such as thin dendritic branches and spines, with sub-micrometric precision.

Most *in vivo* studies have been performed in 1P widefield illumination, resulting already in important advances towards the understanding of neuronal circuit activity under physiological and pathological conditions, as well as the link between cellular mechanisms and behavior (Gradinaru et al., 2007; Sohal et al., 2009; Tsai et al., 2009; Kravitz et al., 2010). However the high spatial and temporal specificity provided by 2PE, together with the possibility to penetrate deep into living tissues, would be a fundamental advantage.

Here we reviewed the latest optical illumination methods used to address the challenging issue of 2PE of optogenetic tools. In particular, the low conductivity of

optogenetic channels was overcome by scanning a low-NA laser spot through the target excitation area (Rickgauer and Tank 2009; Andrasfalvy et al., 2010), or by using phase modulation techniques (TF-DH or TF-GPC), which shape the excitation beam to generate axially resolved extended light patterns (Papagiakoumou et al., 2010). Despite these recent works, the greatest part of 2P photoactivation studies has been carried out, so far, by photolysis of caged neurotransmitters, since photolysis is more easily induced by 2P diffraction-limited spots (Carter and Sabatini 2004; Nikolenko et al., 2007; Losonczy et al., 2008; Branco et al., 2010). In particular, recently, simultaneous 2P photolysis and Ca^{2+}imaging were demonstrated by combining a holographic setup for glutamate uncaging and a galvo-steered for imaging system or *vice versa* (Dal Maschio et al., 2010). A sufficiently high SNR was achieved in both cases, even though the number of frames per second recorded was limited by the necessity to efficiently excite the fluorophore.

Similar setups could be used for combined functional imaging and photoavtivation of optogenetic tools, thus advancing our understanding on the functioning of neuronal networks at cellular or subcellular level. However, information is still missing on the 2P cross sections of optogenetic tools. So far, to our knowledge, only 2P cross section of ChR2 has been measured (Rickgauer and Tank 2009), owing probably to the fact that ChR2, is the first discovered and the most widely used optogenetic tool for photoactivation. But the development of other types of opsins (Halorhodopsin, *NpHR*, Volvox-carteri channelrhodopsins, *VChR1-2*, ultrafast channelrhodopsin, *ChETA*, etc.) (Gradinaru et al., 2007; Lin 2011), that can target different cell populations and are activated in different wavelength regions, thus enabling parallel studies of different networks, moves really fast. Thus, for further development of 2P optogenetics, an extensive study of the 2P properties of these proteins is needed. Similar studies are needed for VSDs and VSFPs, which could also benefit from the use of depth-resolved large excitation areas. Especially in the case of VSDs, the lack of genetic specificity makes the need for axial confinement even more important.

Concerning parallel illumination methods, further improvements may be necessary to alternate multiple excitation patterns into the preparation at a rate > 100 Hz, in order to mimic rapidly changing neuronal activity patterns. For both GPC and DH, the phase profiles addressed to the SLM can be calculated in advance, in order to reduce as much as possible the computation time. In this case, the refresh rate of the SLM becomes the limiting factor. Typical nematic LC matrices that are used for

phase modulation in applications like DH (entire interval 0-2π of phase range) are limited to a refresh rate of 60 Hz, but new nematic LCs operating at 200 Hz are now appearing on the market.

Another interesting possibility to be explored would be the use of ferroelectric liquid crystal matrices, binary SLMs (phase delay either 0 or π), which can operate at rates >1 kHz. This would be straightforward with GPC, since this technique only requires a binary phase modulation, contrary to DH. However, ferroelectric LC-SLMs suffer from low diffraction efficiency, as we already mentioned, which is far below the theoretical maximum of 40% (Golan et al., 2009), making, thus, these devices a poor choice for 2P excitation, where available power at the sample is often a limiting factor. Future improvements, however, might render this technology applicable to 2P patterned illumination.

Acknowledgements

DO acknowledges support by the European Research Council starting investigator grant SINSLIM and the Crown center of photonics. EP was supported by the "Fondation pour la Recherche Médicale" (FRM). FA was supported by the European doctoral school Frontières du Vivant. FA and VE were supported by the "Fondation pour la Recherche Médicale" (FRM équipe) and by the Human Frontier Science Program (RGP0013/2010).

References

Akemann, W., Mutoh, H., Perron, A., Rossier, J. and Knopfel, T. (2010). Imaging brain electric signals with genetically targeted voltage-sensitive fluorescent proteins. *Nat Methods*, 7, pp. 643-649.

Andrasfalvy, B. K., Zemelman, B. V., Tang, J. and Vaziri, A. (2010). Two-photon single-cell optogenetic control of neuronal activity by sculpted light. *Proc Natl Acad Sci U S A*, 107, pp. 11981-11986.

Anselmi, F., Ventalon, C., Begue, A., Ogden, D. and Emiliani, V. (2011). 3D imaging and photostimulation by remote focusing and holographic light patterning, *Proc Natl Acad Sci U S A* 108, 19504-19509.

Aravanis, A. M., Wang, L. P., Zhang, F., Meltzer, L. A., Mogri, M. Z., Schneider, M. B., et al. (2007). An optical neural interface: in vivo control of rodent motor cortex with integrated fiberoptic and optogenetic technology. *J Neural Eng*, 4, pp. S143-156.

Arenkiel, B. R., Peca, J., Davison, I. G., Feliciano, C., Deisseroth, K., Augustine, G. J., et al. (2007). In vivo light-induced activation of neural circuitry in transgenic mice expressing channelrhodopsin-2. *Neuron*, 54, pp. 205-218.

Botcherby, E.J., Juskaitis, R., Booth, M.J. & Wilson, T. (2007).Aberration-free optical refocusing in high numerical aperture microscopy. *Optics Letters*, 32, 2007-2009.

Botcherby, E. J., Smith, C. W., Booth, M. J., Juskaitis, R. and Wilson, T. (2010). Arbitrary-scan imaging for two-photon microscopy. *Proc. of SPIE*, 756917, pp. 1-8.

Branco, T., Clark, B. A. and Hausser, M. (2010). Dendritic discrimination of temporal input sequences in cortical neurons. *Science*, 329, pp. 1671-1675.

Cardin, J. A., Carlen, M., Meletis, K., Knoblich, U., Zhang, F., Deisseroth, K., et al. (2009). Driving fast-spiking cells induces gamma rhythm and controls sensory responses. *Nature*, 459, pp. 663-667.

Carter, A. G. and Sabatini, B. L. (2004). State-dependent calcium signaling in dendritic spines of striatal medium spiny neurons. *Neuron*, 44, pp. 483-493.

Chanda, B., Blunck, R., Faria, L. C., Schweizer, F. E., Mody, I. and Bezanilla, F. (2005). A hybrid approach to measuring electrical activity in genetically specified neurons. *Nat Neurosci*, 8, pp. 1619-1626.

Curtis, J. E., Koss, B. A. and Grier, D. G. (2002). Dynamic holographic optical tweezers. *Opt. Communi.*, 207, pp. 169.

Dal Maschio, M., De Stasi, A. M., Benfenati, F. and Fellin, T. (2011). Three dimensional in vivo scanning microscopy with inertia-free focus control *Optics Letters*, 36, pp. 3503-3505.

Dal Maschio, M., Difato, F., Beltramo, R., Blau, A., Benfenati, F. and Fellin, T. (2010). Simultaneous two-photon imaging and photo-stimulation with structured light illumination. *Optics Express*, 18, pp. 18720-18731.

Dana, H. and Shoham, S. (2011). Numerical evaluation of temporal focusing characteristics in transparent and scattering media *Opt Express*, 19, pp. 4937-4948.

Daria, V. R., Stricker, C., Bowman, R., Redman, S. and Bachor, H. A. (2009). Arbitrary multisite two-photon excitation in four dimensions. *Applied Physics Letters*, 95, pp. 093701.

Dhawale, A. K., Hagiwara, A., Bhalla, U. S., Murthy, V. N. and Albeanu, D. F. (2010). Non-redundant odor coding by sister mitral cells revealed by light addressable glomeruli in the mouse. *Nat Neurosci*, 13, pp. 1404-1412.

Di Leonardo, R., Ianni, F. and Ruocco, G. (2007). Computer generation of optimal holograms for optical trap arrays. *Optics Express*, 15, pp. 1913-1922.

Du, R., Bi, K., Zeng, S., Li, D., Xue, S., & Luo, Q. (2009). Analysis of fast axial scanning scheme using temporal focusing with acousto-optic deflectors. *Journal of Modern Optics*, *56*, 81-84.

Durst, M. E., Zhu, G. & Xu, C. (2008).Simultaneous spatial and temporal focusing in nonlinear microscopy. *Optics Communications*, *281*, 1796-1805 .

Durst, M. E., Zhu, G. and Xu, C. (2006). Simultaneous spatial and temporal focusing for axial scanning. *Opt. Express*, 14, pp. 12243-12254.

Emiliani, V., Cojoc, D., Ferrari, E., Garbin, V., Durieux, C., Di Fabrizio, E., et al. (2006). Wavefront engineering microscopy to study 3D mechanotransduction in living cells. *Proc. SPIE* 6195 pp. 61950J

Farah, N., Reutsky, I. and Shoham, S. (2007). Patterned optical activation of retinal ganglion cells. *Conf Proc IEEE Eng Med Biol Soc*, 2007, pp. 6369-6371.

Feldbauer, K., Zimmermann, D., Pintschovius, V., Spitz, J., Bamann, C. and Bamberg, E. (2009). Channelrhodopsin-2 is a leaky proton pump. *Proc Natl Acad Sci U S A*, 106, pp. 12317-12322.

Fisher, J. A., Barchi, J. R., Welle, C. G., Kim, G. H., Kosterin, P., Obaid, A. L., et al. (2008). Two-photon excitation of potentiometric probes enables optical recording of action potentials from mammalian nerve terminals in situ. *J Neurophysiol*, 99, pp. 1545-1553.

Fisher, J. A., Salzberg, B. M., Yodh, A. G. (2005).Near infrared two-photon excitation cross-sections of voltage-sensitive dyes. *Journal of Neuroscience Methods, 148*, 94-102.

Fricke, M. and Nielsen, T. (2005). Two-dimensional imaging without scanning by multifocal multiphoton microscopy. *Appl Opt*, 44, pp. 2984-2988.

Gerchberg, R. W. and Saxton, W. O. (1972). A pratical algorithm for the determination of the phase from image and diffraction pictures. *Optik*, 35, pp. 237-246.

Glückstad, J. (1996). Phase contrast image synthesis. *Opt.Commun*, 130, pp. 225.

Glückstad, J. and Mogensen, P. C. (2001). Optimal phase contrast in common-path interferometry. *Appl Opt*, 40, pp. 268-282.

Golan, L., Reutsky, I., Farah, N. and Shoham, S. (2009). Design and characteristics of holographic neural photo-stimulation systems. *J Neural Eng*, 6, pp. 66004.

Golan, L. and Shoham, S. (2009). Speckle elimination using shift-averaging in high-rate holographic projection. *Opt Express*, 17, pp. 1330-1339.

Goodman, J. W. (2005). Introduction to Fourier Optics, 3rd Edition. New York.

Gradinaru, V., Mogri, M., Thompson, K. R., Henderson, J. M. and Deisseroth, K. (2009). Optical deconstruction of parkinsonian neural circuitry. *Science*, 324, pp. 354-359.

Gradinaru, V., Thompson, K. R., Zhang, F., Mogri, M., Kay, K., Schneider, M. B., et al. (2007). Targeting and readout strategies for fast optical neural control in vitro and in vivo. *J Neurosci*, 27, pp. 14231-14238.

Grossman, N., Poher, V., Grubb, M. S., Kennedy, G. T., Nikolic, K., McGovern, B., et al. (2010). Multi-site optical excitation using ChR2 and micro-LED array. *J Neural Eng*, 7, pp. 16004.

Judkewitz, B., Roth, A. and Hausser, M. (2006). Dendritic enlightenment: using patterned two-photon uncaging to reveal the secrets of the brain's smallest dendrites. *Neuron*, 50, pp. 180-183.

Kramer, R. H., Fortin, D. L. and Trauner, D. (2009). New photochemical tools for controlling neuronal activity. *Curr Opin Neurobiol*, 19, pp. 544-552.

Kravitz, A. V., Freeze, B. S., Parker, P. R., Kay, K., Thwin, M. T., Deisseroth, K., et al. (2010). Regulation of parkinsonian motor behaviours by optogenetic control of basal ganglia circuitry. *Nature*, 466, pp. 622-626.

Kuhn, B., Denk, W. and Bruno, R. M. (2008). In vivo two-photon voltage-sensitive dye imaging reveals top-down control of cortical layers 1 and 2 during wakefulness. *Proc Natl Acad Sci U S A*, 105, pp. 7588-7593.

Kwon, H. B. and Sabatini, B. L. (2011). Glutamate induces de novo growth of functional spines in developing cortex. *Nature*, 474, pp. 100-104.

Leach, J., Wulff, K., Sinclair, G., Jordan, P., Courtial, J., Thomson, L., et al. (2006). Interactive approach to optical tweezers control. *Appl Opt*, 45, pp. 897.

Liesener, J., Reicherter, M., Haist, T. and Tiziani, H. J. (2000). Multi-functional optical tweezers using computer-generated holograms. *Optics Communications*, 185, pp. 77–82.

Lin, J. Y. (2011). A user's guide to channelrhodopsin variants: features, limitations and future developments. *Exp Physiol*, 96, pp. 19-25.

Losonczy, A., Makara, J. K. and Magee, J. C. (2008). Compartmentalized dendritic plasticity and input feature storage in neurons. *Nature*, 452, pp. 436-441.

Losonczy, A., Zemelman, B. V., Vaziri, A. and Magee, J. C. (2010). Network mechanisms of theta related neuronal activity in hippocampal CA1 pyramidal neurons. *Nat Neurosci*, 13, pp. 967-972.

Lutz, C., Otis, T. S., de Sars, V., Charpak, S., DiGregorio, D. A. and Emiliani, V. (2008). Holographic photolysis of caged neurotransmitters. *Nat Methods*, 5, pp. 821-827.

Mutoh, H., Perron, A., Akemann, W., Iwamoto, Y. and Knopfel, T. (2011). Optogenetic monitoring of membrane potentials. *Exp Physiol*, 96, pp. 13-18.

Nikolenko, V., Peterka, D. S. and Yuste, R. (2010). A portable laser photostimulation and imaging microscope. *J Neural Eng*, 7, pp. 045001.

Nikolenko, V., Poskanzer, K. E. and Yuste, R. (2007). Two-photon photostimulation and imaging of neural circuits. *Nat Methods*, 4, pp. 943-950.

Nikolenko, V., Watson, B. O., Araya, R., Woodruff, A., Peterka, D. S. and Yuste, R. (2008). SLM Microscopy: Scanless Two-Photon Imaging and Photostimulation with Spatial Light Modulators. *Front Neural Circuits*, 2, pp. 1-14.

Oron, D. and Silberberg, Y. (2005). Harmonic generation with temporally focused ultrashort pulses. *J. Opt. Soc. Am. B*, 22, pp. 2660-2663.

Oron, D., Tal, E. and Silberberg, Y. (2005). Scanningless depth-resolved microscopy. *Opt. Express*, 13, pp. 1468-1476.

Palima, D. and Glückstad, J. (2008). Multi-wavelength spatial light shaping using generalized phase contrast. *Optics Express*, 16, pp. 1331-1342.

Papagiakoumou, E., Anselmi, F., Bègue, A., de Sars, V., Gluckstad, J., Isacoff, E. Y., et al. (2010). Scanless two-photon excitation of channelrhodopsin-2. *Nat Methods*, 7, pp. 848-854.

Papagiakoumou, E., de Sars, V., Emiliani, V. and Oron, D. (2009). Temporal focusing with spatially modulated excitation. *Optics Express*, 17, pp. 5391-5401.

Papagiakoumou, E., de Sars, V., Oron, D. and Emiliani, V. (2008). Patterned two-photon illumination by spatiotemporal shaping of ultrashort pulses. *Optics Express*, 16, pp. 22039-22047.

Peterka, D. S., Takahashi, H. and Yuste, R. (2011). Imaging voltage in neurons. *Neuron*, 69, pp. 9-21.

Petreanu, L., Huber, D., Sobczyk, A. and Svoboda, K. (2007). Channelrhodopsin-2-assisted circuit mapping of long-range callosal projections. *Nat Neurosci*, 10, pp. 663-668.

Petreanu, L., Mao, T., Sternson, S. M. and Svoboda, K. (2009). The subcellular organization of neocortical excitatory connections. *Nature*, 457, pp. 1142-1145.

Reicherter, M., Haist, T., Wagemann, E. U. and Tiziani, H. J. (1999). Optical particle trapping with computer-generated holograms written on a liquid-crystal display. *Opt Lett*, 24, pp. 608-610.

Rhodes, W. T., Ed. (2009). Generalized Phase Contrast. Application in Optics and Photonics. Atlanta, Springer.

Rickgauer, J. P. and Tank, D. W. (2009). Two-photon excitation of channelrhodopsin-2 at saturation. *Proceedings of the National Academy of Sciences of the United States of America*, 106, pp. 15025-15030.

Rodrigo, P. J., Daria, V. R. and Glückstad, J. (2004). Real-time three-dimensional optical micromanipulation of multiple particles and living cells. *Opt Lett*, 29, pp. 2270-2272.

Salter, P. S., Carbone, G., Botcherby, E. J., Wilson, T., Elston, S. J. and Raynes, E. P. (2009). Liquid crystal director dynamics imaged using two-photon fluorescence microscopy with remote focusing. *Phys Rev Lett*, 103, pp. 257803.

Sohal, V. S., Zhang, F., Yizhar, O. and Deisseroth, K. (2009). Parvalbumin neurons and gamma rhythms enhance cortical circuit performance. *Nature*, 459, pp. 698-702.

Straub, A., Durst, M. E. and Xu, C. (2011). High speed multiphoton axial scanning through an optical fiber in a remotely scanned temporal focusing setup. *Biomed Opt Express*, 2, pp. 80-88.

Suchowski, H., Oron, D., Silberberg, Y. (2006). Generation of a dark nonlinear focus by spatio-temporal coherent control. *Opt. Communications*, 264, pp. 482-487.

Tal, E., Oron, D. and Silberberg, Y. (2005). Improved depth resolution in video-rate line-scanning multiphoton microscopy using temporal focusing. *Opt Lett*, 30, pp. 1686-1688.

Theer, P. and Denk, W. (2006). On the fundamental imaging-depth limit in two-photon microscopy. *J Opt Soc Am A Opt Image Sci Vis*, 23, pp. 3139-3149.

Tsai, H. C., Zhang, F., Adamantidis, A., Stuber, G. D., Bonci, A., de Lecea, L., et al. (2009). Phasic firing in dopaminergic neurons is sufficient for behavioral conditioning. *Science*, 324, pp. 1080-1084.

Vaziri, A. and Emiliani, V. (2011). *Curr Opin Neurobiol*, in press.

Wang, H., Peca, J., Matsuzaki, M., Matsuzaki, K., Noguchi, J., Qiu, L., et al. (2007). High-speed mapping of synaptic connectivity using photostimulation in Channelrhodopsin-2 transgenic mice. *Proc Natl Acad Sci U S A*, 104, pp. 8143-8148.

Witten, I. B., Lin, S. C., Brodsky, M., Prakash, R., Diester, I., Anikeeva, P., et al. (2010). Cholinergic interneurons control local circuit activity and cocaine conditioning. *Science*, 330, pp. 1677-1681.

Wyart, C., Del Bene, F., Warp, E., Scott, E. K., Trauner, D., Baier, H., et al. (2009). Optogenetic dissection of a behavioural module in the vertebrate spinal cord. *Nature*, 461, pp. 407-410.

Yang, S., Papagiakoumou, E., Guillon, M., de Sars, V., Tang, C. M. and Emiliani, V. (2011). Three-dimensional holographic photostimulation of the dendritic arbor. *J Neural Eng*, 8, pp. 046002.

Zahid, M., Velez-Fort, M., Papagiakoumou, E., Ventalon, C., Angulo, M. C. and Emiliani, V. (2010). Holographic photolysis for multiple cell stimulation in mouse hippocampal slices. *PLoS One*, 5, pp. e9431.

Zernike, F. (1955). How I Discovered Phase Contrast. *Science*, 121, pp. 345-349.

Zhu, G., van Howe, J., Durst, M., Zipfel, W. and Xu, C. (2005). Simultaneous spatial and temporal focusing of femtosecond pulses. *Opt Express*, 13, pp. 2153-2159.

Figure Legends

Fig. 1: *First demonstration of action potential generation by 2P activation of ChR2 in neurons.* a) Schematic depiction of geometry of whole-cell scanning 2PE, shown in side and top view. b) Measured 2P intensity profiles of the Point Spread Function (PSF) at several effective NA values, along the optical axis *z* (top) and in the lateral (*x*-*y*) plane (bottom). c) Current-clamp recordings of membrane voltage changes, stimulated by using 32-ms spiral scans with a 2PE spot with PSF corresponding to the case of NA = 0.3. Overline indicates stimulation time. Adapted from (Rickgauer and Tank 2009).

Fig. 2: *Digital holography.* a) Diagram of the experimental scheme for DH. b) Block diagram of the iterative Fourier transform algorithm (Gerchberg and Saxton algorithm) for calculating the phase-hologram addressed to the SLM.

Fig. 3: *Multispot generation.* a) Schematic diagram and phase hologram for displacing the spots laterally (left panel), axially (middle panel) and both laterally and axially (right panel) by imposing a grating effect, lens effect and combined grating and lens effect, respectively to the phase hologram. At the bottom of each panel a description of the phase function is given for each case, in relation to the spatial coordinates x_h, y_h at the back focal plane of the objective lens. a and a' are constants, u_n is the amplitude of the n^{th} spot and mod 2π stands for 2π modulation. b) Holographic diffraction-limited spots placed in two (left panel) and three dimensions (right panel) by using a grating and lenses and a GSW algorithm, respectively. Spots are visualized by exciting fluorescence on a thin fluorescent film by 2PE (left) and 1PE (right) (adapted from Yang et al., 2011). On the left panel the fluorescence of the spots was superimposed to the fluorescence image of a Purkinje cell.

Figure 4: *Holographic excitation.* a) Layout of the experimental setup for DH. By designing the target intensity profile on the base of the fluorescence picture, light excitation can be shaped to perfectly match: b) a specific subcellular process (adapted from Lutz et al., 2008 and Papagiakoumou et al., 2008) and c) a cell soma, a defined group of cells or the extracellular space (adapted from Zahid et al., 2010).

Figure 5: *Axial resolution of holographic spots.* Axial propagations measured in a range of 100 µm around the focal plane of the objective for a) a 20-µm-FWHM Gaussian beam, b) a 20-µm holographic spot in 1P excitation (axial resolution of 33 µm at FWHM) and c) a 20-µm holographic spot in 2PE (axial resolution of 25 µm at FWHM). In each case the corresponding phase profile at the back aperture of the objective and the *x*-*y* intensity profile at the sample plane are shown.

Figure 6: *Patterned excitation for glutamate uncaging.* a) 2P uncaging of MNI-glutamate performed simultaneously on cerebellar granule cells in culture (targeted cells are marked by red lines) with the image mask shown on the left, generated to shape the laser wave front of the uncaging beam. Imaging is performed, simultaneously to uncaging, with conventional scanning microscopy at 0.54 Hz. The time course of $\Delta F/F_0$ values of Fluo-4 fluorescence in the 7 ROIs denoted in the fluorescence image with green, before and after the application of the holographic

uncaging stimulus, are shown on the right. The arrows indicate the time of delivery of the photolysis stimulus (0.26 mW/μm^2) (adapted from (Dal Maschio et al., 2010)). b) SLM multi-spot imaging of Ca^{2+} transients induced by 2P uncaging of glutamate to activate cortical neurons in brain slices. After detection of the ROIs (red contours) on the fluorescence image of labeled neurons (obtained with conventional raster scanning), pixel centers of mass of each ROI are calculated, and their coordinates are used as a command image uploaded to the SLM software. The SLM illuminates all or a subset of the ROIs and a widefield detector, with spatial resolution suitable to resolve individually illuminated objects, is used to record neuronal activity from all illuminated neurons simultaneously (adapted from (Nikolenko et al., 2008)). c) Variations of intracellular Ca^{2+} concentration of two different target CA1 hippocampal neurons (1 & 2 on the fluorescence image) during 1P uncaging of MNI-glutalate with the pattern configuration of the inset (adapted from (Zahid et al., 2010)).

Figure 7: *The Generalized Phase Contrast method.* a) Optical setup for the GPC (adapted from (Palima and Glückstad 2008)) and layout of the corresponding experimental setup. b) Shaped laser patterns generated with the GPC method (2PE) designed on the basis of a confocal fluorescence image of a Purkinje cell (up) and a widefield fluorescence image of CA1 hippocampal neurons loaded with oregon green bapta (down), in selected ROIs (white line) (adapted from (Papagiakoumou et al., 2010)). c) *y-z* section of the measured axial propagation of a 20-μm-diameter spot, generated with GPC in 2PE. Note the diffraction pattern rising from the interference of the signal wave with the reference wave component.

Figure 8: *Temporal focusing.* The standard setup for temporal focusing consists of a grating, placed at one end of a 2f-2f telescope comprised of an achromatic lens of focal length f_1 and an objective lens of effective focal length f_2 placed at a distance f_1+f_2 from one another. The ultrashort pulse impinges on the grating at an angle α such that the center wavelength is diffracted perpendicular to the grating, towards the optical axis of the lens system. As can be seen, only a thin line is instantaneously illuminated on the grating as the pancake-shaped ultrashort pulse crosses it.

Figure 9: *Temporal focusing combined with spatial light patterning.* a) Layout of the experimental implementation of the GPC technique in combination with TF. b) *y-z* section of the measured axial propagation of a 20-μm-temporally focused

holographic spot (left panel) and a 20-μm-GPC-generated temporally focused spot. The axial distribution of the integrated fluorescence intensity on the area of the spots is plotted on the diagram shown (adapted from (Papagiakoumou et al., 2010)).

Figure 10: *TF-GPC enables efficient 2P excitation of ChR2 in brain slices.* a) Excitation (0.3-0.5 mW/μm^2) of layer V pyramidal neurons, ChR2-YFP positive, in cortical slices with temporally focused GPC spots of 15 μm with a 2-ms light stimulation (top), with 10-ms light stimulation in different firing frequencies (middle) and by simultaneous photoactivation(10-ms light pulses) of two neurons (bottom). In each case the neurons responded reliably to the stimulation by action potentials. b) Fluorescence image of a neuron filled with Alexa Fluor 594 with superimposed shaped excitation profile covering the apical dendrite (red; top). Photo-depolarizations evoked by the excitation shape (0.3 mW/μm^2) with a 10-ms light stimulation at different z-axis positions (bottom). Adapted from (Papagiakoumou et al., 2010).

Figure 11: *Decoupling the imaging from the photoactivation plane.* a) Representation of the generation of multiple holographic spots at axial positions different from the objective's focal plane, by projecting different phase holograms each one introducing a variable lens effect that cancels the defocusing of the objective (adapted from (Emiliani et al., 2006)). b) Schematic layout of the experimental setup permitting the displacement of the temporal focus plane position (z_{TF}). Introducing GVD to the original laser beam results to a quadratically curved wavefront at the Fourier plane of the TF telescope, which displaces the temporal focus plane in the axial direction, depending on the amount of the GVD. c) Schematic layout of a remote focusing setup. Excitation spots (red dots) are placed into the sample through the principal objective (left). A perfect 3D image of the sample is recreated after the remote objective (right). A mirror in the remote space moves this image (right, blue and green) in respect to the focal plane of the remote objective, in order to select the final imaging plane on the camera, which can be axially displaced (left, blue and green dotted lines) from the principal focal plane of the microscope (left, dashed gray line). The position of the principal objective (and so, of the excitation spots) is not affected by remote focusing.

Figure 12: *In depth two-photon excitation.* a) 2P-excited fluorescence images on a thin fluorescent film of: (a) a 15-μm diameter spot generated with GPC, (b) a

configuration of multiple spots of 7-µm diameter and (c) a holographic pattern mimicking the neuron with its small processes, without scattering (no slice; left) and after propagation through acute cortical brain slices of 550 µm with TF (middle) and without TF in the optical setup (right). 2P fluorescence was excited at λ=950nm, with a 60x, 0.9 NA, objective lens.

Tables

Table 1: *Summary of the illumination techniques for 2P-photoactivation*

	Spiral scanning	***Scanning and TF***	***DH and TF***	***GPC and TF***
Implementation	*Conventional 2P microscope*	*2P microscope +grating for TF*	*2P microscope +setup for DH and grating for TF*	*2P microscope +setup for GPC and grating for TF*
Max excitation density	Laser power/w_0	Laser power/A_{spot} 15-20% at grating	Laser power/A_{spot} 15-20% at grating 30% at SLM	¼ Laser power/FOV 15-20% at grating
FOV *(for 40x objective)*	$\left(2 \cdot f_{scan} \cdot tg(\vartheta)\frac{f_{obj}}{f}\right)^2$ ~600x600µm^2	$\left(2 \cdot f_{scan} \cdot tg(\vartheta)\frac{f_{obj}}{f}\right)^2$ ~600x600µm^2	$\left[2 \times \left((\lambda f_{obj} f_1)/(2d_{SLM} f_2)\right)\right]^2$ ~120x120µm^2 (@ 900 nm)	$\pi \cdot \left(Rc \cdot \frac{f_2}{f_1}\frac{f_{obj}}{f}\right)^2$ R_c~100µm^2
Diffraction efficiency	constant	constant	$\propto \left(\frac{\sin X}{X}\right)^4$	$\delta_\eta\left(\frac{r}{\Delta R}\right) \cdot 4 \cdot \frac{A_{spot}}{\mathrm{FOV}}$
Axial resolution	$\propto \frac{\pi w_0^2}{2\lambda} \cong \frac{\lambda}{\mathrm{NA}^2}$	$\propto \frac{2f^2}{k(s^2+\alpha^2\Omega^2)} \cong \frac{\lambda}{\mathrm{NA}}$	$\propto \frac{2f^2}{k(s^2+\alpha^2\Omega^2)} \cong \frac{\lambda}{\mathrm{NA}_{obj}^2}$	$\propto \frac{2f^2}{k(s^2+\alpha^2\Omega^2)} \cong \frac{\lambda}{\mathrm{NA}_{\mathrm{obj}}^2}$
Temporal resolution	$T_S = N(t_{dwell} + S_t)$	$T_S = N(t_{dwell} + S_t)$	t_{dwell}	t_{dwell}
Temporal resolution *or sequential patterning*	$T_S = N(t_{dwell} + S_t)$	$T_S = N(t_{dwell} + S_t)$	$t_{dwell} + 1/R_e$	$t_{dwell} + 1/R_e$

(a)

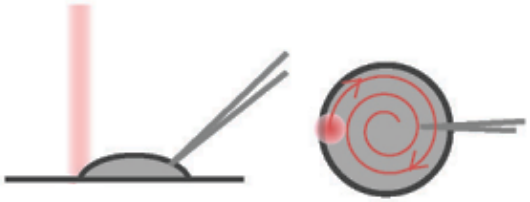

Spiral scanning

(b)

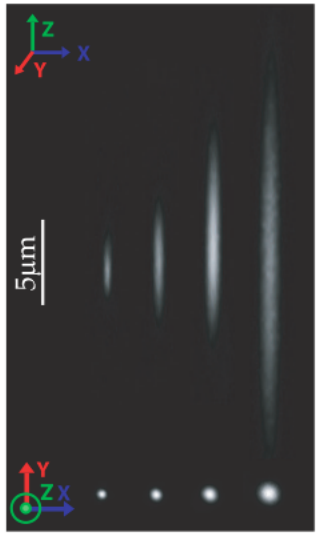

(c)

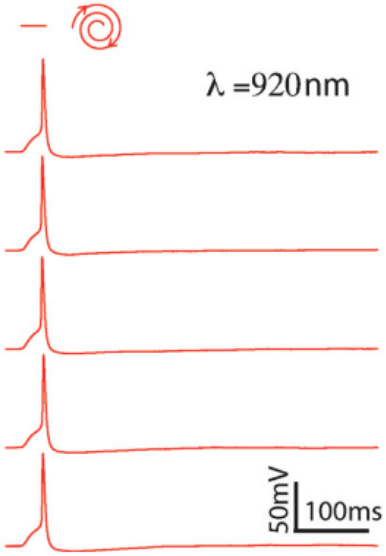

Figure 1

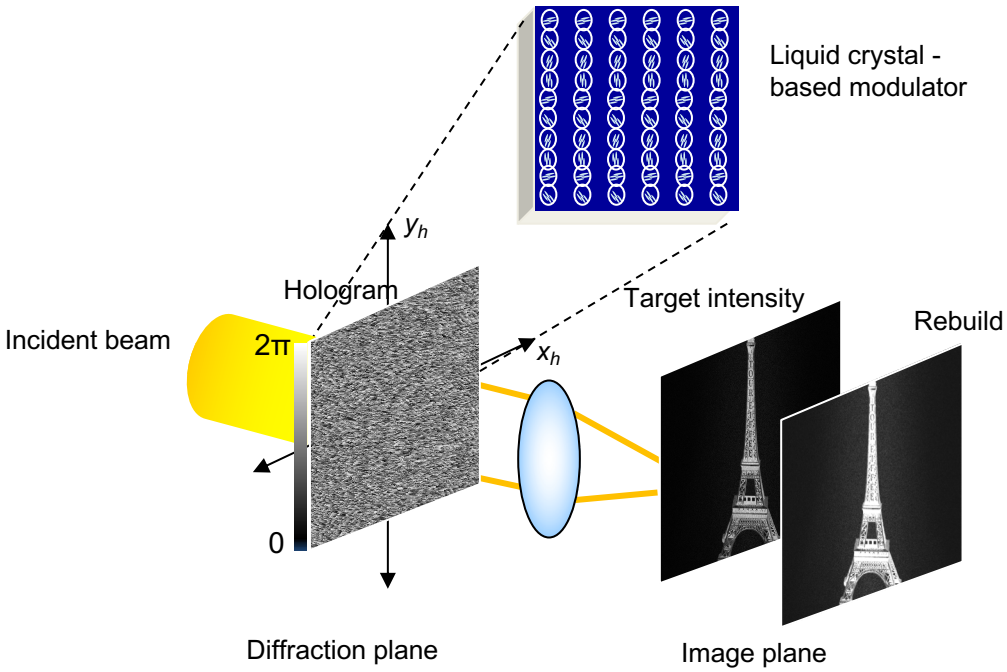
Liquid crystal -
based modulator
y_h
Hologram
Target intensity
Rebuild
Incident beam
2π
x_h
0
Diffraction plane
Image plane

Figure 2a

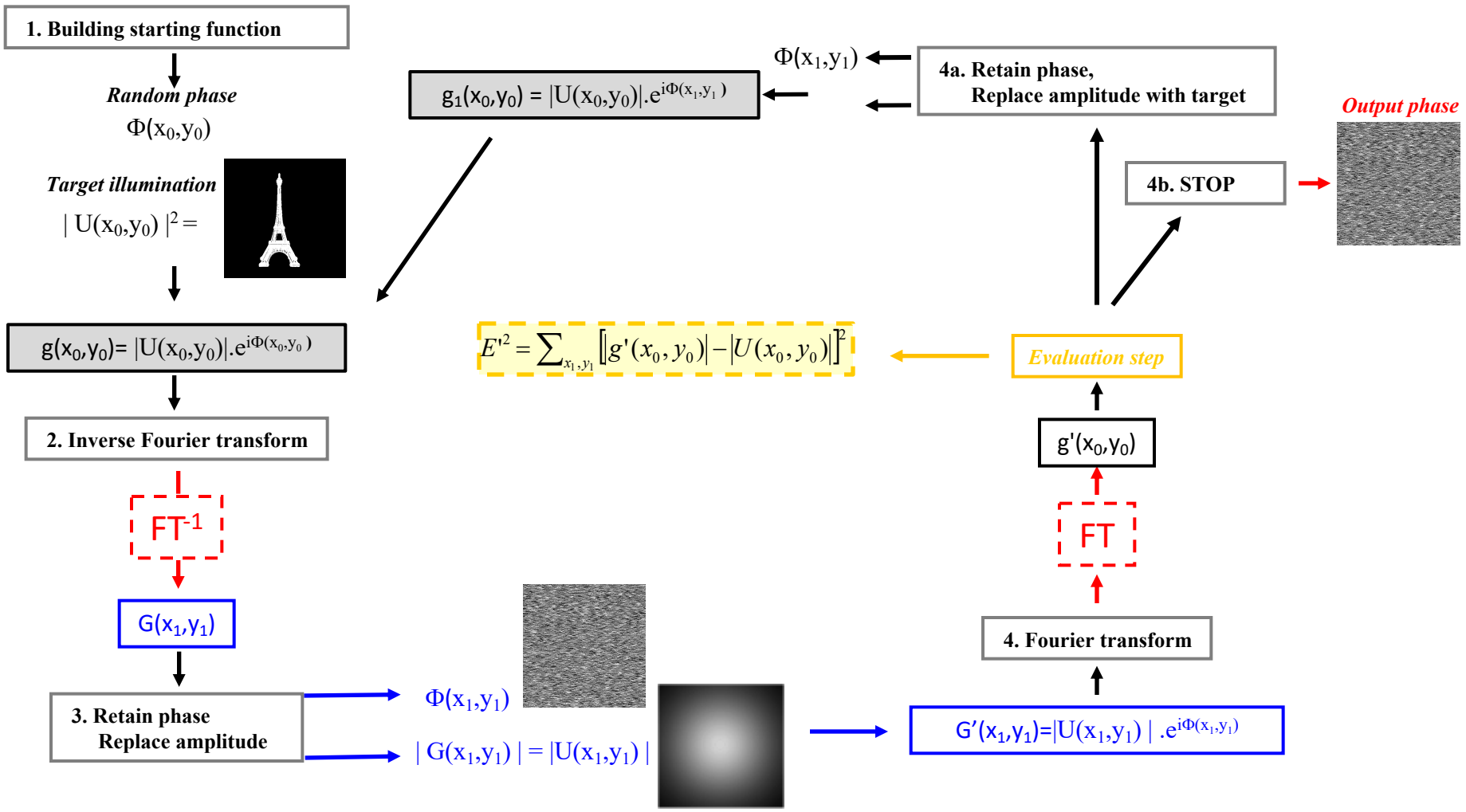
1. Building starting function
Random phase
Φ(x0,y0)
Target illumination
| U(x0,y0) |2 =
g(x0,y0)= |U(x0,y0)|.eiΦ(x0,y0)
2. Inverse Fourier transform
FT-1
G(x1,y1)
3. Retain phase
Replace amplitude
Φ(x1,y1)
| G(x1,y1) | = |U(x1,y1) |
G'(x1,y1)=|U(x1,y1) | .eiΦ(x1,y1)
4. Fourier transform
FT
g'(x0,y0)
Evaluation step
E'2 = ∑x1,y1 [|g'(x0,y0)| − |U(x0,y0)|]2
g1(x0,y0) = |U(x0,y0)|.eiΦ(x1,y1)
Φ(x1,y1)
4a. Retain phase,
Replace amplitude with target
4b. STOP
Output phase

Figure 2b

(a)

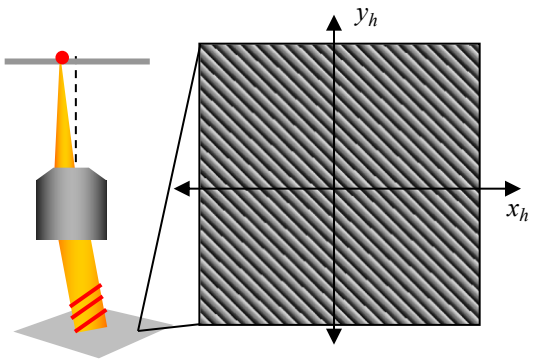

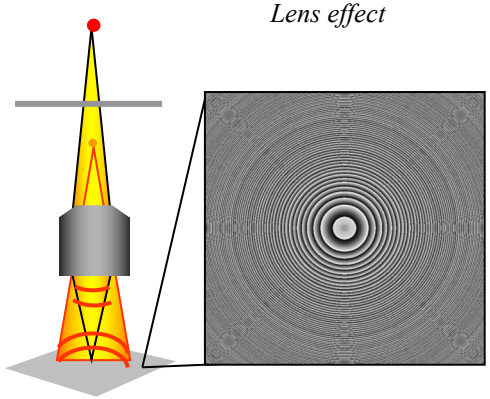

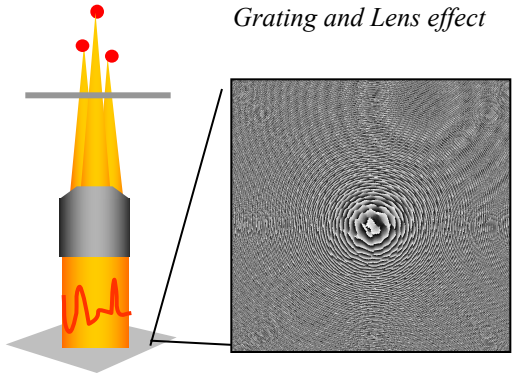

$$\phi_{grating}(x_h, y_h) = a\left(x_h \cdot \Delta x + y_h \cdot \Delta y\right) \bmod 2\pi$$

$$\phi_{lens}(x_h, y_h) = a' \cdot \Delta z\left({x_h}^2 + {y_h}^2\right) \bmod 2\pi$$

$$\phi_{tot} = \arg\left(\sum_{n=1}^{N} u_n e^{i(\phi_{grating} + \phi_{lens})_n}\right) \bmod 2\pi$$

(b)

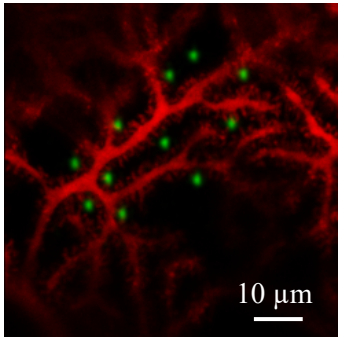

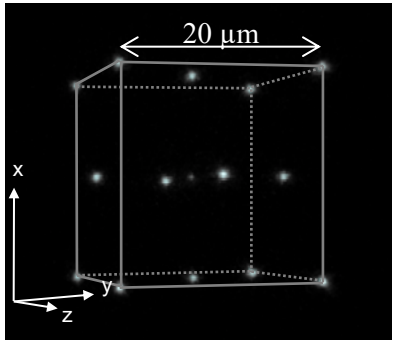

Figure 3

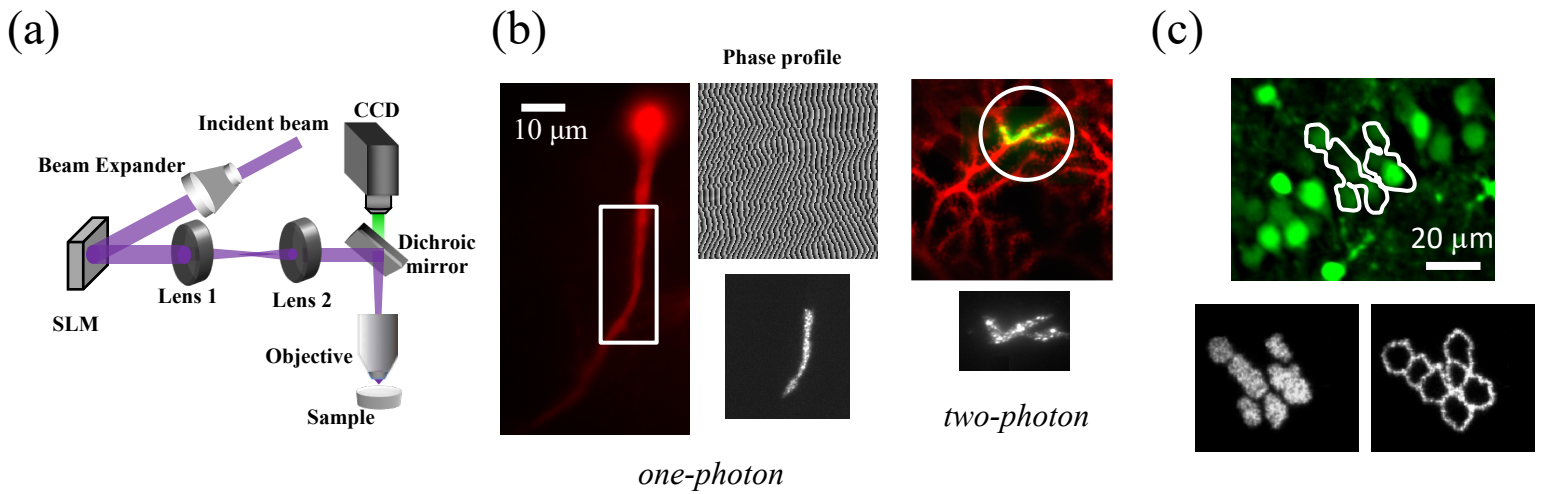
(a)
Incident beam
CCD
Beam Expander
Dichroic mirror
Lens 1
Lens 2
SLM
Objective
Sample
(b)
Phase profile
10 µm
one-photon
two-photon
(c)
20 µm

Figure 4

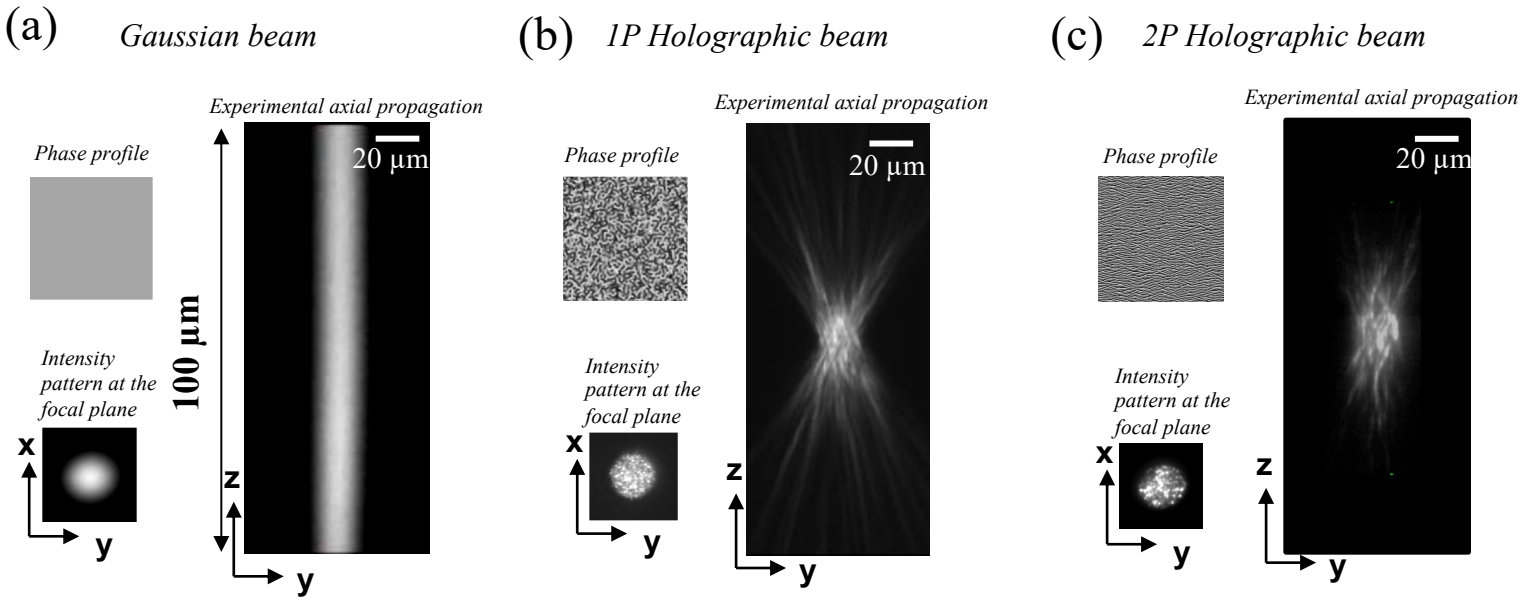
(a)
Gaussian beam
Phase profile
Intensity pattern at the focal plane
x
y
Experimental axial propagation
100 µm
z
y
20 µm
(b)
1P Holographic beam
Phase profile
Intensity pattern at the focal plane
x
y
Experimental axial propagation
z
y
20 µm
(c)
2P Holographic beam
Phase profile
Intensity pattern at the focal plane
x
y
Experimental axial propagation
z
y
20 µm

Figure 5

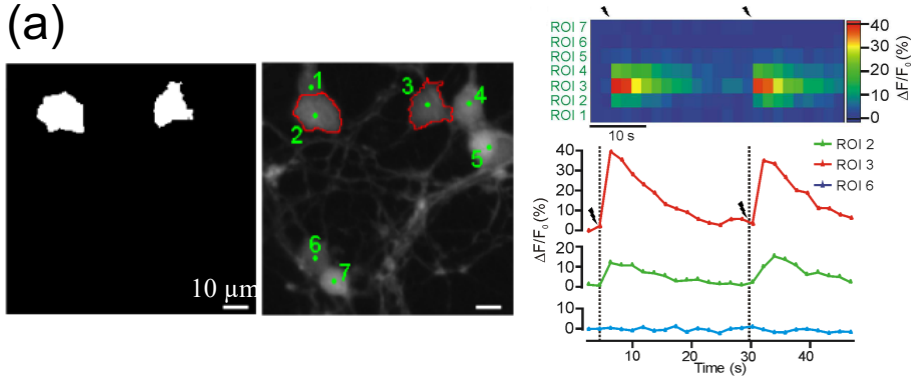
(a)
10 µm
1
2
3
4
5
6
7
ROI 7
ROI 6
ROI 5
ROI 4
ROI 3
ROI 2
ROI 1
40
30
20
10
0
ΔF/F0 (%)
10 s
ROI 2
ROI 3
ROI 6
Time (s)

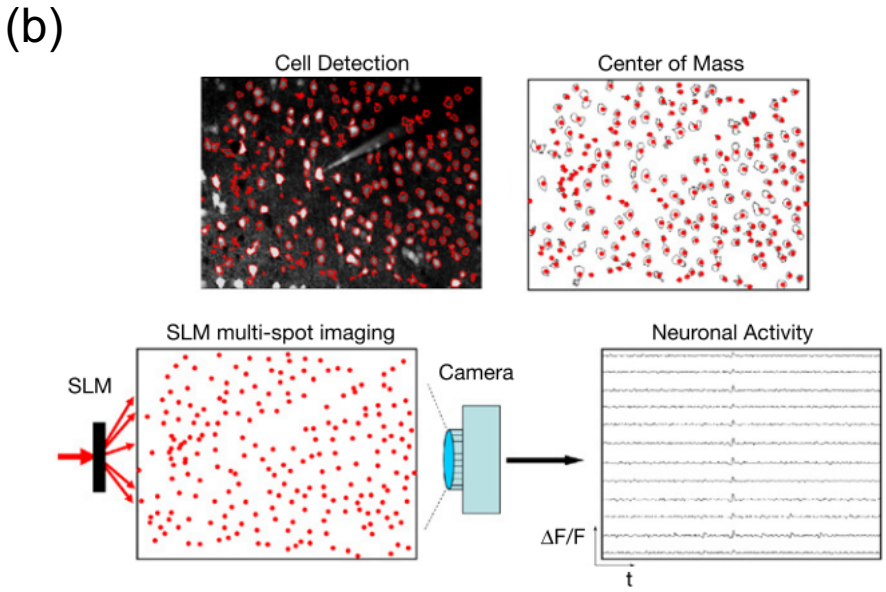
(b)
Cell Detection
Center of Mass
SLM multi-spot imaging
SLM
Camera
Neuronal Activity
ΔF/F
t

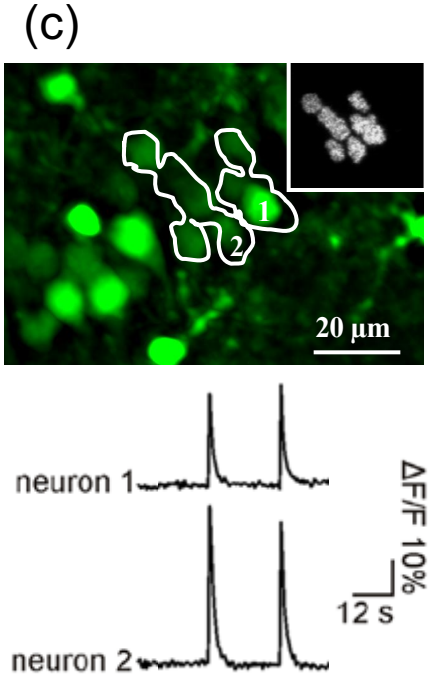
(c)
1
2
20 µm
neuron 1
neuron 2
ΔF/F 10%
12 s

Figure 6

(a)

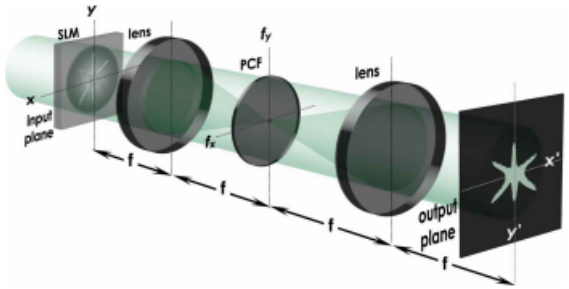
y
SLM
lens
f_y
PCF
lens
x
input plane
f_x
x'
f
f
f
output plane
y'
f

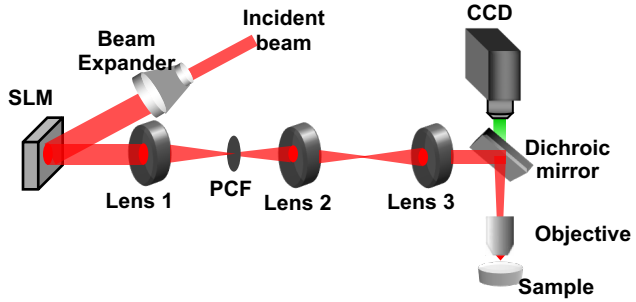
Incident beam
Beam Expander
CCD
SLM
Dichroic mirror
Lens 1
PCF
Lens 2
Lens 3
Objective
Sample

(b)

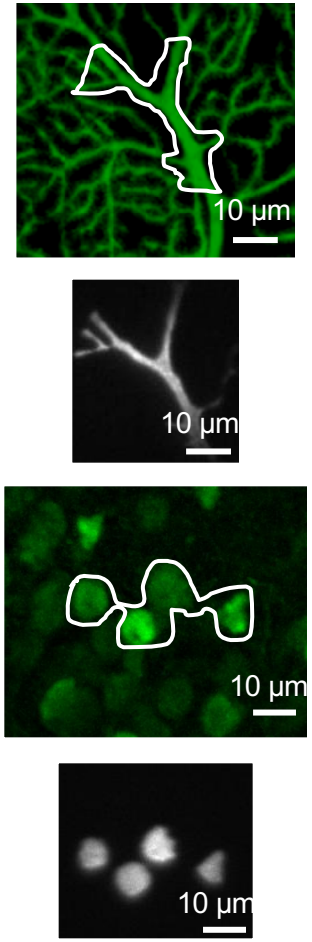
10 µm
10 µm
10 µm
10 µm

(c)

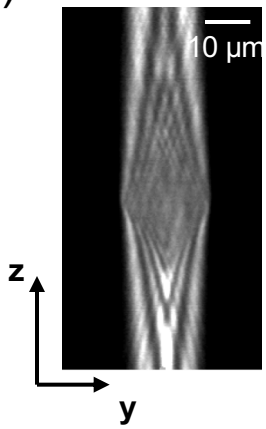
10 µm
z
y

Figure 7

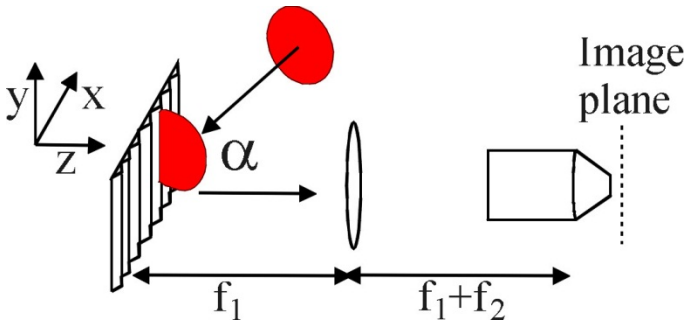

Figure 8

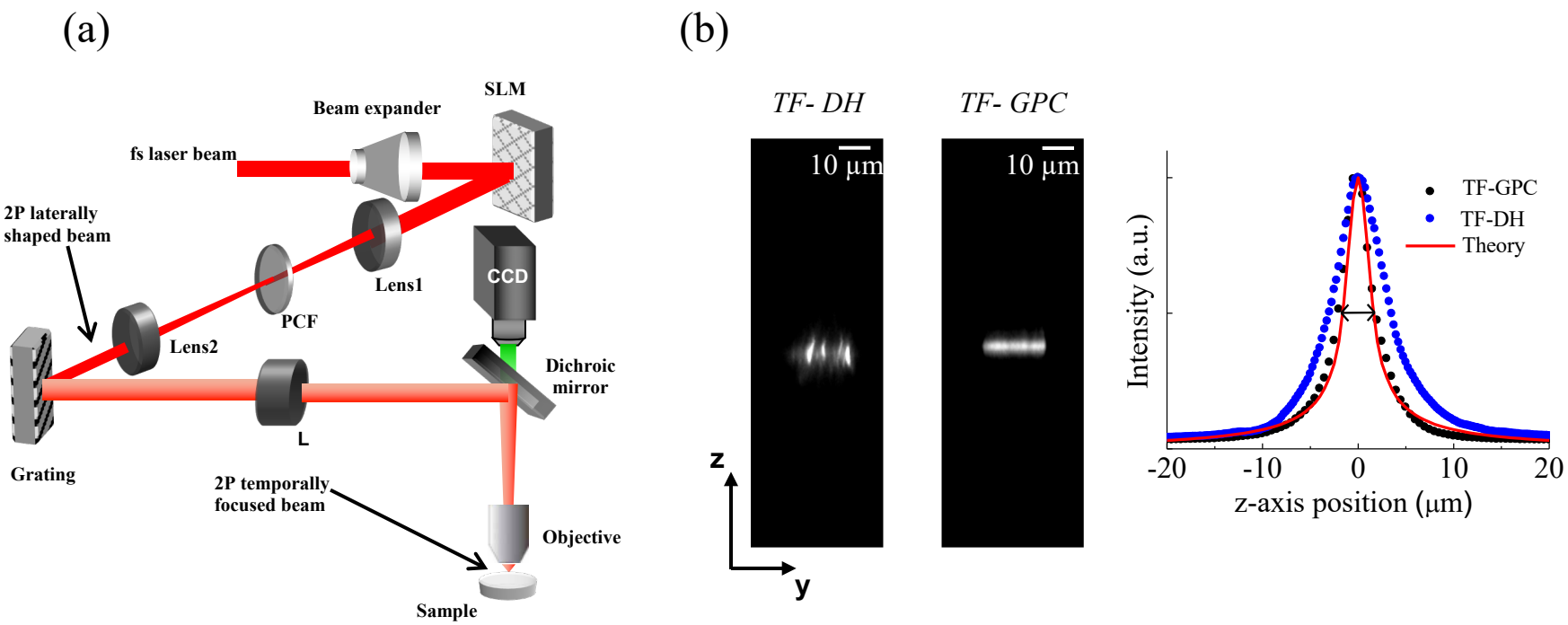
(a)
SLM
Beam expander
fs laser beam
2P laterally
shaped beam
Lens1
CCD
PCF
Lens2
Dichroic
mirror
L
Grating
2P temporally
focused beam
Objective
Sample
(b)
TF- DH
TF- GPC
10 μm
10 μm
z
y
TF-GPC
TF-DH
Theory
Intensity (a.u.)
-20
-10
0
10
20
z-axis position (μm)

Figure 9

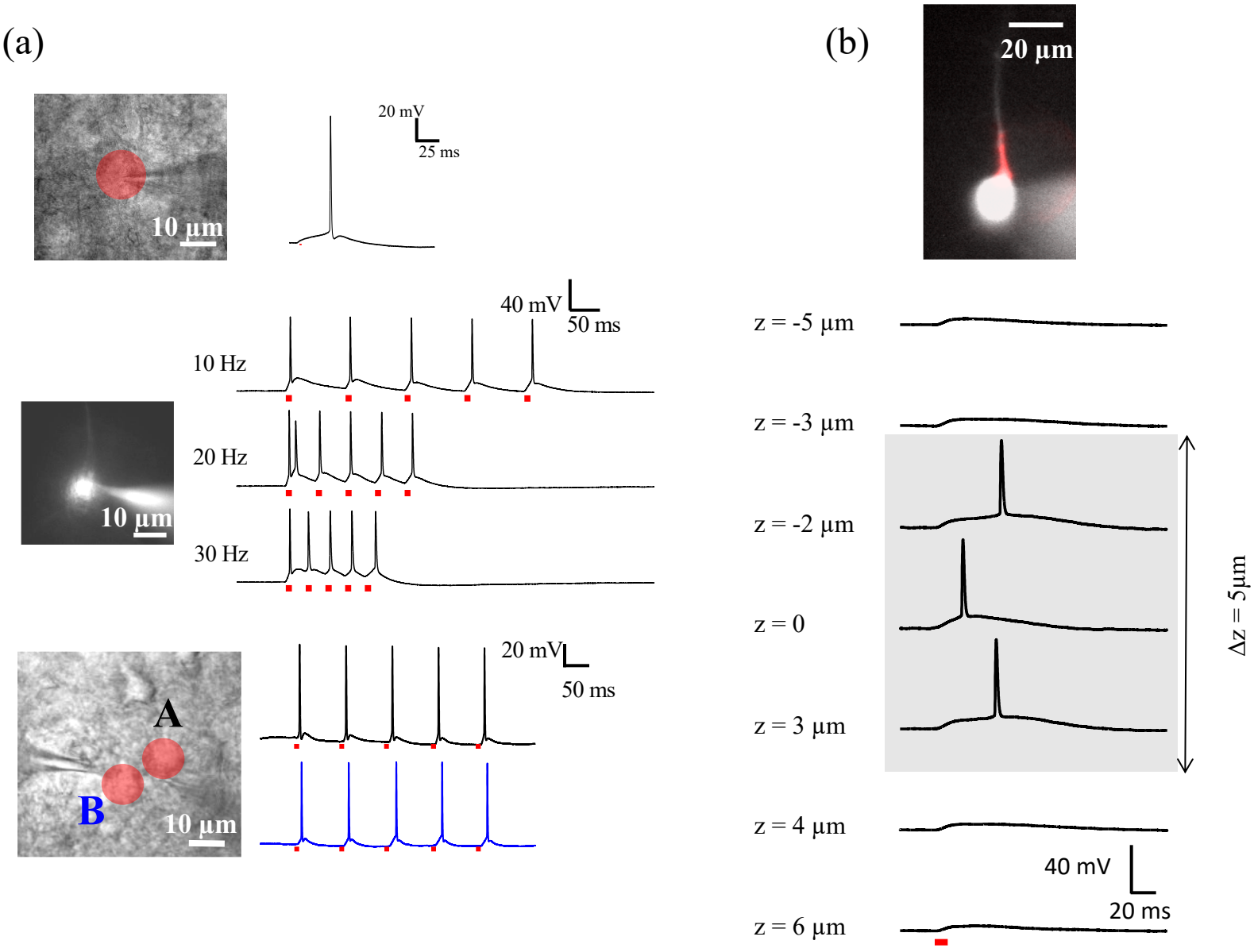
(a)
10 µm
20 mV
25 ms
40 mV
50 ms
10 Hz
20 Hz
30 Hz
10 µm
20 mV
50 ms
A
B
10 µm
(b)
20 µm
z = -5 µm
z = -3 µm
z = -2 µm
z = 0
z = 3 µm
z = 4 µm
z = 6 µm
Δz = 5µm
40 mV
20 ms

Figure 10

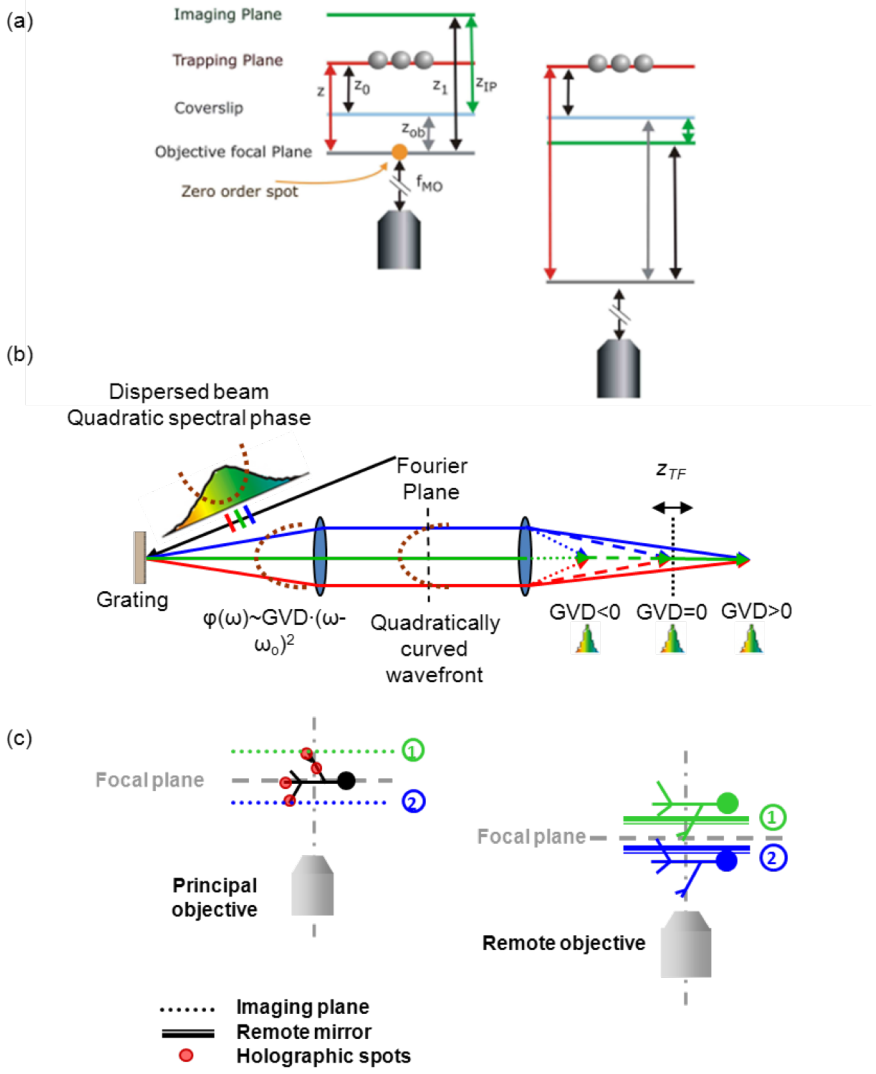
(a)
Imaging Plane
Trapping Plane
Coverslip
Objective focal Plane
Zero order spot
z
z_0
z_1
z_{IP}
z_{ob}
f_{MO}
(b)
Dispersed beam
Quadratic spectral phase
Fourier Plane
z_{TF}
Grating
φ(ω)~GVD·(ω-ω$_o$)^2
Quadratically curved wavefront
GVD<0
GVD=0
GVD>0
(c)
Focal plane
Principal objective
Focal plane
Remote objective
Imaging plane
Remote mirror
Holographic spots

Figure 11

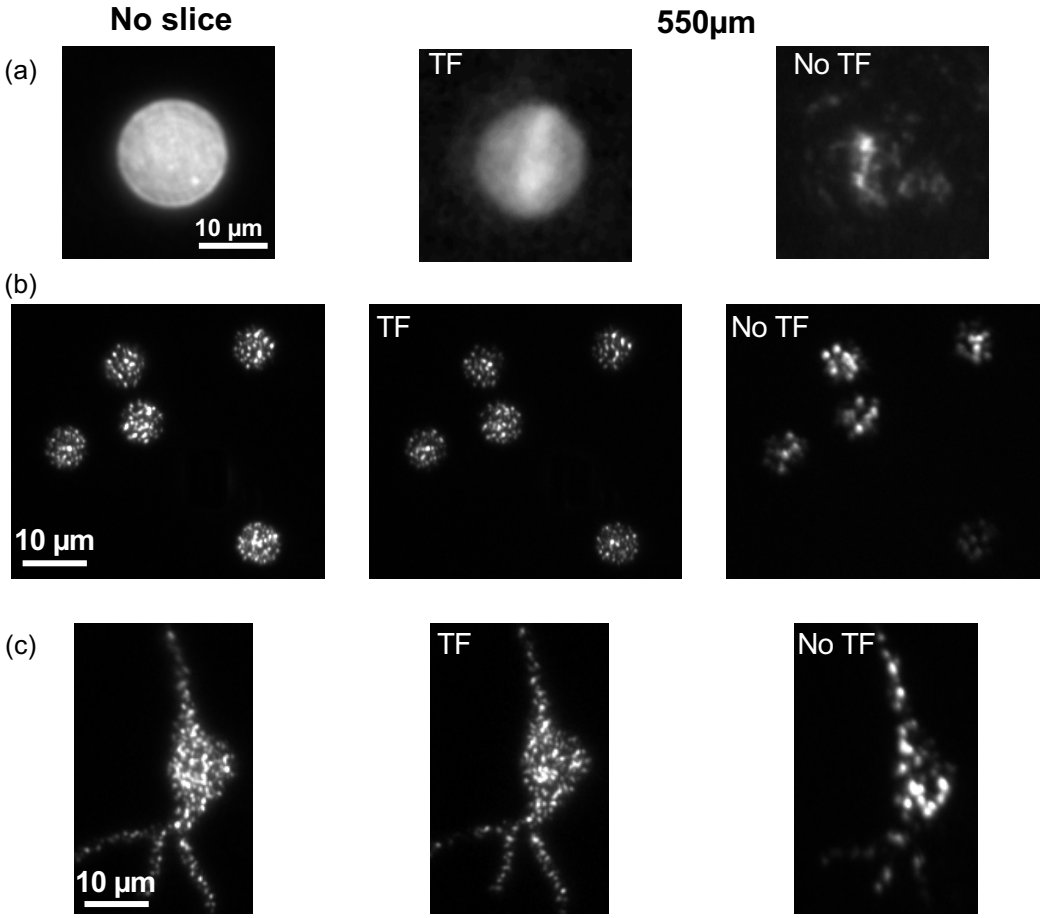

Fig.12: *In depth two-photon excitation.* 2P-excited fluorescence images on a thin fluorescent film of: a) a 15-µm diameter spot generated with GPC, (b) a configuration of multiple spots of 7-µm diameter and (c) a holographic pattern mimicking the neuron with its small processes, without scattering (no slice; left) and after propagation through acute cortical brain slices of 550 µm with TF (middle) and without TF in the optical setup (right). 2P fluorescence was excited at λ=950 nm, with a 60x, 0.9 NA , objective lens.

Figure 12